40th Fluid Dynamics Conference and Exhibit
28 June - 1 July 2010, Chicago, Illinois

AIAA 2010-4483

Asymptotic Methods for Solving Wave Propagation Problems in Porous Tubes, Channels and Spheres

Joseph Majdalani*
University of Tennessee Space Institute, Tullahoma, TN 37388

We consider the general boundary-value ODE that describes the wave motion inside porous tubes, channels, and spheres. Its corresponding physical problem is simultaneously dispersive and dissipative, exhibiting both oscillatory and damped behavior. The attendant second order equation is controlled by two keystone parameters: ε, the inverse of the cross-flow Reynolds number, and S, the Strouhal number. The presence of a third parameter λ is also entertained. In this work, asymptotic solutions are obtained using WKB, composite-scaling (CST), and generalized-scaling (GST) techniques. The last two methods are based on multiple-scale theory and lead to additional physical insight into the nonlinear scaling structure that characterizes the ensuing wave motion. The GST approach remains unique in that it obviates the need for guesswork or rationalization. Accordingly, the inner scales are deduced from the problem's solvability condition. This procedure enables us to solve problems which were hitherto difficult or intractable by conventional multiple-scale expansions. By way of illustration, three examples are provided. In addition to being conjecture-free, the one-term GST solution is simple to derive, compact, of nearly second order in ε, and capable of pinpointing the problem's nonlinear scales. The CST's main advantage lies in its minimal integrability requirement. In this work, two simple proofs are provided to show that the keystone CST scale, which is used at the basis of the composite-scaling technique, does indeed return the problem's inner and outer variable transformations in their respective regions of applicability.

I. Introduction

THE purpose of this paper is threefold. First, it is to present, in general conceptual form, some of the fundamental asymptotic solutions for viscous wave propagation inside porous enclosures using a conventional Wentzel, Kramers, and Brillouin (WKB) approach. Second, it serves to illustrate the application of the composite-scaling technique (CST) to the same problem. The CST approach was discussed by Majdalani[1] and Majdalani and Van Moorhem[2] in the context of an oscillatory flow in a tube with transpiring walls. Therein, its outcome was scrutinized by means of numerical and experimental verifications. The method was subsequently applied in the modeling of internal flows in porous channels and cavities by several workers. These include Majdalani and Roh,[3] Majdalani,[4,5] Wasistho, Balachandar and Moser,[6] and Chedevergne, Casalis, and Majdalani.[7] CST is a variant of multiple-scale and matched-asymptotic expansions that may be useful in the treatment of problems that exhibit an underlying multiple-scale structure. As such, it can be suitable in the mathematical modeling of internal combustion and unsteady flows in porous enclosures where the interplay of dissimilar physical mechanisms can evolve at several disparate scales.[6-14] In general, it may apply to unsteady convection-diffusion equations in which both dispersive and dissipative mechanisms co-exist.

From matched-asymptotic expansions, CST borrows the concept of constructing a composite scale, instead of a composite solution, that can reproduce or match asymptotically the inner and outer scales, instead of the inner and outer solutions, in their respective domains. Its novelty lies in the idea of matching scales, instead of solutions, that are legitimate inner and outer approximations.

---

*H. H. Arnold Chair of Excellence in Advanced Propulsion, Mechanical, Aerospace and Biomedical Engineering Department. Senior Member AIAA. Fellow ASME.

The third goal of this investigation is to discuss a conceptual scheme that is hoped to broaden the scope of multiple-scale expansions. Its originality stands in the manner by which a generalized expression for the inner scales can be obtained directly from the problem's solvability condition.[15] Unlike the CST's procedural requirement of defining the scales at the beginning of analysis, the third approach operates with a generalized-scaling variable that is left unspecified during the derivation process. In contrast to traditional multiple-scale methods that rely on foreknowledge of the inner transformations, the generalized-scaling variable will be determined by imposing the problem's solvability condition. As such, closure is deduced from the mathematical need for boundedness between successive perturbation levels. The so-called generalized-scaling technique (GST)[16] precludes the known pitfalls and elements of uncertainty that are often associated with traditional modes of selecting scales (e.g., via conjecture, inspection, rationalization, or trial). It is stricter to formulate initially due to the need to retain generality. But once constructed, the GST solution offers the freedom to accommodate the particular transformation that is germane to the problem's underlying multiple-scale structure.[16] Furthermore, it will be shown to outperform, in some cases, two of the formerly presented solutions. In addition to the novelty in obtaining the scale *a posteriori*, the GST's main contribution lies in the manner by which retaining an inner transformation in conceptual form can be combined with the mathematical requirement for boundedness to arrive at a uniformly valid solution.

The boundary-value problem to be solved entails a singular, second-order, ordinary differential equation (ODE) seeded with two perturbation parameters. The equation represents the cross-flow component of the linearized rotational momentum equation that appears in the analysis of oscillatory fluid motions inside viscous channels, tubes, or spheres with permeable walls.[1-5,15-19] It is obtained from the Navier-Stokes equations via perturbations in the small pressure wave amplitude. The so-called wave amplitude denotes the ratio of the oscillatory amplitude and the mean pressure inside the enclosure in question. The presence of several scales is commensurate with the multiple time-dependent inertial, convective, and diffusive mechanisms that stem from inevitable mean-flow interactions with the oscillatory wave motion.

Technically, the paper is organized as follows. To begin, a WKB solution is derived for the generalized cross-flow momentum equation in porous channels, tubes, and spheres. This is followed by a presentation of the alternative CST approach. The latter is used to identify the intrinsically nonlinear scaling structure. The GST approach is presented last. A practical example is then chosen for which an exact solution can be arrived at. Two more examples are discussed for which only asymptotic solutions may be obtained. Results from both asymptotic and exact predictions are compared and analyzed. The special examples that we address emerge from practical applications. Similar equations arise in a variety of problems involving both theoretical[1-5,15-19] and computational[6-14] models of burning propellant, hydrodynamic instability of oscillatory flows,[20-27] isotope separation,[28-31] and ultrafiltration.[32]

II. Problem Formulation

We introduce the rotational cross-flow boundary-layer equation for small-amplitude pressure perturbations in a porous enclosure. In studies addressing simple geometric settings,[1-5] this equation has been shown to exhibit the general form

$$\varepsilon y'' + \left[a_0(x) + \varepsilon a_1(x)\right] y' + \left[b_0(x) + \varepsilon b_1(x) + iSc_0(x)\right] y = 0; \quad a_0(0) = 0 \tag{1}$$

$$y'(0) = 0, \qquad y(1) = 1 \tag{2}$$

In Eq. (1), the x-coordinate represents the dimensionless normal/radial distance measured from the core ($x = 0$) to the porous walls ($x = 1$). Additionally, $i = \sqrt{-1}$, and a_0, a_1, b_0, b_1, and c_0 are real coefficients. The case considered here corresponds to inflow across the walls for which $a_0(x) > 0, \quad x \in]0,1]$.

The leading term ε conveys the reciprocal of the cross-flow Reynolds number, $R = Vh/\nu$. Due to small viscosity, most practical applications excluding some biological flows and flows inside microchannels correspond to $R \geq 10$.[33] The additional presence of unsteadiness is materialized in the appearance of the Strouhal number, $S = \omega h / V$. For nontrivial oscillations, $S \geq 10$, thus introducing a secondary perturbation parameter. Inasmuch as R and S are independent, their ratio, $S/R = (V_D/V)^2$ scales with the quotient of the small diffusion speed ($V_D = \sqrt{\omega\nu}$) and the convection speed through the sidewalls (V). For nontrivial injection, $V_D \leq V$ and $S \leq R$. As usual, ω, ν, and h are the circular frequency, kinematic viscosity, and core-to-wall distance. In view of $1 < S \leq R$, it is reasonable to define ε and S to be the small (primary) and large (secondary) perturbation parameters, respectively. If $S = \mathcal{O}(\varepsilon^{-q})$, physical conditions translate into $1 < S \leq \varepsilon^{-1}$, or $0 < q \leq 1$. In addition to the uniformly valid order $q = \frac{1}{2}$, a special situation can be associated with the limiting order $q = 1$ for which $S = \mathcal{O}(R)$.

Because of symmetry about the core, $a_0(0)=0$ satisfies the physical requirement of a vanishing normal/radial component of the velocity.[28] It also gives rise to a regular singularity.

III. On the WKB Technique

Following Bender and Orszag,[34] a WKB solution can be sought via

$$y(x)=\exp\left(\delta^{-1}p_0+p_1+\delta p_2+\delta^2 p_3+\delta^3 p_4+\ldots\right) \tag{3}$$

where δ is a small parameter and $p_j(x)$ ($j\in\mathbb{Z}^+$) are to be determined. Differentiation gives

$$y'=(\delta^{-1}p_0'+p_1'+\delta p_2'+\delta^2 p_3'+\delta^3 p_4'+\ldots)y \tag{4}$$

$$\begin{aligned}y''=\Big[&\delta^{-2}p_0'^2+\delta^{-1}(p_0''+2p_0'p_1')+p_1''+p_1'^2+2p_0'p_2'+\delta(p_2''+2p_0'p_3'+2p_1'p_2')\\&+\delta^2(p_3''+p_2'^2+2p_0'p_4'+2p_1'p_3')+\ldots\Big]y\end{aligned} \tag{5}$$

When Eqs. (3)-(5) are substituted into Eq. (1), the resulting equation can be multiplied by δ and rearranged into

$$\begin{aligned}&\varepsilon\left[\delta^{-1}p_0'^2+p_0''+2p_0'p_1'+\delta(p_1''+p_1'^2+2p_0'p_2')+\delta^2(p_2''+2p_0'p_3'+2p_1'p_2')+\ldots\right]\\&+(a_0+\varepsilon a_1)(p_0'+\delta p_1'+\delta^2 p_2'+\delta^3 p_3'+\ldots)+\delta(b_0+\varepsilon b_1)+iS\delta c_0=0\end{aligned} \tag{6}$$

At least two possible distinguished limits are possible, depending on the order of S.

A. Type I: $R\sim S^2$

For a typical physical setting associated with an injection-induced flow, $S=\mathcal{O}(\varepsilon^{-1/2})$ or $R=\mathcal{O}(S^2)$. The corresponding large cross-flow Reynolds number translates into a deeply penetrating wave that decays rather slowly, thus justifying the under-damped characterization. When similar quantities in Eq. (6) are grouped in descending order, one obtains

$$\begin{aligned}&\left[iS\delta c_0+a_0p_0'\right]+\delta\left[\varepsilon\delta^{-2}p_0'^2+a_0p_1'+b_0\right]+\delta^2\left[\varepsilon\delta^{-2}(p_0''+2p_0'p_1'+a_1p_0')+a_0p_2'\right]\\&+\delta^3\left[\varepsilon\delta^{-2}(p_1''+p_1'^2+2p_0'p_2'+a_1p_1'+b_1)+a_0p_3'\right]+\mathcal{O}(\delta^4,\varepsilon\delta^2)\equiv 0,\quad\forall\delta\end{aligned} \tag{7}$$

The distinguished limit must be prescribed in a manner to allow terms between brackets to display the same order. By inspection, this condition will be true when $\varepsilon\delta^{-2}=\mathcal{O}(1)$ and $S\delta=\mathcal{O}(1)$. Both requirements are satisfied when $\delta=\mathcal{O}(\varepsilon^{1/2})$ and $S=\mathcal{O}(\varepsilon^{-1/2})$. Without loss of generality, we choose the distinguished limit to be $\delta=\varepsilon^{1/2}$ and substitute this back into Eq. (7). At the outset, the defining equations for $p_j(x)$ can be produced in succession (by collecting terms that are of the same order in $\varepsilon^{1/2}$). The zero-order equation becomes

$$a_0p_0'+iS\sqrt{\varepsilon}c_0=0,\qquad p_0=-iS\sqrt{\varepsilon}\int_1^x c_0a_0^{-1}\mathrm{d}t \tag{8}$$

Similarly, terms of $\mathcal{O}(1)$ yield

$$p_0'^2+a_0p_1'+b_0=0,\qquad p_1=\int_1^x\left(-b_0a_0^{-1}+\varepsilon S^2c_0^2a_0^{-3}\right)\mathrm{d}t \tag{9}$$

At $\mathcal{O}(\sqrt{\varepsilon})$, the equation in p_2' reads $p_0''+2p_0'p_1'+a_1p_0'+a_0p_2'=0$. Thus, we retrieve

$$p_2=iS\sqrt{\varepsilon}\int_1^x\left[\left(a_0c_0'+a_0a_1c_0-c_0a_0'-2b_0c_0\right)a_0^{-3}+2\varepsilon S^2c_0^3a_0^{-5}\right]\mathrm{d}t \tag{10}$$

Higher corrections may be obtained at orders ε and $\varepsilon^{3/2}$ from $a_0p_3'+p_1'^2+2p_0'p_2'+p_1''+a_1p_1'+b_1=0$ and, consecutively, $a_0p_4'+p_2''+2p_0'p_3'+2p_1'p_2'+a_1p_2'=0$. These produce

$$\begin{aligned}p_3=\int_1^x\Big[&\left(a_0b_0'+a_0a_1b_0-a_0^2b_1-b_0a_0'-b_0^2\right)a_0^{-3}\\&+\varepsilon S^2\left(6c_0^2b_0+5c_0^2a_0'-4a_0c_0c_0'-3c_0^2a_0^2a_1\right)a_0^{-5}-5\varepsilon^2S^4c_0^4a_0^{-7}\Big]\mathrm{d}t\end{aligned} \tag{11}$$

$$\begin{aligned}p_4=iS\sqrt{\varepsilon}\int_1^x\Big[&\left(3a_0a_0'c_0'+6a_0a_1b_0c_0+4a_0b_0c_0'+3c_0a_0a_1a_0'+c_0a_0a_0''+4a_0c_0b_0'-10b_0c_0a_0'-6b_0^2c_0-3c_0a_0'^2\right.\\&\left.-2a_0^2a_1c_0'-a_0^2a_1^2c_0-a_0^2c_0''-a_0^2a_0'c_0'-2a_0^2b_1c_0\right)a_0^{-5}-14\varepsilon^2S^4c_0^5a_0^{-9}\\&+\varepsilon S^2\left(22c_0^3a_0'+20b_0c_0^3-16a_0c_0^2c_0'-10c_0^3a_0a_1\right)a_0^{-7}\Big]\mathrm{d}t\end{aligned} \tag{12}$$

Letting $w(x)\equiv-\int^x[(b_0+iSc_0)/a_0]\mathrm{d}t$ and $\xi\equiv\varepsilon S^2=\mathcal{O}(1)$, the $\mathcal{O}(\varepsilon)$ solution can be expressed as

$$y_0^{\mathrm{W}}(x)=\exp\left\{w(x)-w(1)+\xi\int_1^x a_0^{-3}\left[c_0^2+iS^{-1}\left(a_0c_0'+a_0a_1c_0-c_0a_0'-2b_0c_0+2\xi c_0^3a_0^{-2}\right)\right]\mathrm{d}t\right\}$$

$$= \exp\left\{-\int_1^x b_0 a_0^{-1}\mathrm{d}t - iS\int_1^x c_0 a_0^{-1}\mathrm{d}t + \xi\int_1^x a_0^{-3}\left[c_0^2 + iS^{-1}\left(a_0 c_0' + a_0 a_1 c_0 - c_0 a_0' - 2b_0 c_0 + 2\xi c_0^3 a_0^{-2}\right)\right]\mathrm{d}t\right\} \tag{13}$$

where the superscript stands for 'WKB' of Type I.

We mention, in passing, that the key similarity parameters that control the solution are S and the viscous damping parameter ξ. It will be later confirmed that the solution type corresponds to a weakly damped oscillatory wave. To obtain y_1^{W} at $\mathcal{O}(\varepsilon^2)$, Eqs. (11) and (12) may be substituted back into Eq. (3). In like manner, higher-order solutions are possible and are best relegated to a symbolic program.

B. Type II: $R \sim S$

For sufficiently small injection, the physical setting for which convection and diffusion velocities meet, $V = \mathcal{O}(V_D)$, corresponds to $S = \mathcal{O}(\varepsilon^{-1})$ or $R = \mathcal{O}(S)$. Overall, this will be the smallest Reynolds number permitted for a fixed Strouhal number. The balance between the cross-flow Reynolds number and the Strouhal number leads to a damped wave. This wave is generally under damped, as with Type I. However, considering that its decay depends on the Strouhal number, the latter, when sufficiently small, leads to a barely oscillatory wave, namely, one that is reminiscent of critically attenuated signals with long wavelengths. Starting again with Eq. (6), quantities of similar order may be grouped sequentially into

$$\begin{aligned}&\left[iS\delta c_0 + a_0 p_0' + p_0'^2\right] + \delta\left[\varepsilon\delta^{-1}(p_0'' + 2p_0'p_1' + a_1 p_0') + a_0 p_1' + b_0\right]\\ &\quad + \delta^2\left[\varepsilon\delta^{-1}(p_1'' + p_1'^2 + 2p_0'p_2' + a_1 p_1' + b_1) + a_0 p_2'\right]\\ &\quad\quad + \delta^3\left[\varepsilon\delta^{-1}(p_2'' + 2p_0'p_3' + 2p_1'p_2' + a_1 p_2') + a_0 p_3'\right] + \mathcal{O}(\delta^4, \varepsilon\delta^3) \equiv 0, \quad \forall\,\delta\end{aligned} \tag{14}$$

Clearly, in order to achieve consistency in asymptotic orders, one should have $\varepsilon\delta^{-1} = \mathcal{O}(1)$ and $S\delta = \mathcal{O}(1)$. Both conditions are satisfied when the distinguished limit is chosen to be $\delta = \varepsilon$. When this order is implemented, the eikonal equation[34] becomes

$$p_0'^2 + a_0 p_0' + iS\varepsilon c_0 = 0, \qquad p_0 = -\tfrac{1}{2}\int_1^x a_0\left(1 \pm \sqrt{1 - 4i\varepsilon S c_0 a_0^{-2}}\right)\mathrm{d}t \tag{15}$$

Since one of the roots corresponds to a left running wave, it yields an unphysical solution that must be eliminated. The meaningful root that we retain is

$$p_0 = -\tfrac{1}{2}\int_1^x a_0\left(1 + \sqrt{1 - 4i\varepsilon S c_0 a_0^{-2}}\right)\mathrm{d}t \tag{16}$$

Next, the transport equation results in

$$(a_0 + 2p_0')p_1' + p_0'' + a_1 p_0' + b_0 = 0, \qquad p_1 = -\int_1^x (p_0'' + a_1 p_0' + b_0)(a_0 + 2p_0')^{-1}\mathrm{d}t \tag{17}$$

A legitimate expansion can now be constructed by combining p_0 and p_1 in Eq. (3). We find

$$y_0^{\mathrm{K}}(x) = \exp\left(\varepsilon^{-1}p_0 + p_1\right) \tag{18}$$

where the superscript K is used to denote a Type II WKB solution ($y^{\mathrm{K}} \equiv y_0^{\mathrm{K}}$). It should be noted that integrating Eq. (16) for arbitrary a_0 and c_0 can at times require computation. Practically, its semi-numerical evaluation can be more intensive than Eq. (8) which, being of lower order in a_0 and c_0, proves to be substantially simpler to process in closed form. This idea will be illustrated in two of the three forthcoming examples.

C. Type III: $R \sim S^3$

Upon further scrutiny, other distinguished limits may be identified. An example includes $\delta = \varepsilon^{1/3}$ for which $\varepsilon = \mathcal{O}(S^{-3})$. This leads to the largest yet cross-flow Reynolds number for a given Strouhal number, $R = \mathcal{O}(S^3)$. The Type III expansion that follows may be expressed in sequential orders of the gauge parameter, $\delta = \varepsilon^{1/3}$. Interestingly, the resulting formulation returns, after four terms are combined, the type I solution evaluated at the same net order in ε. Using the superscript B in reference to this type of solution, one can write at $\mathcal{O}(\varepsilon)$:

$$y_0^{\mathrm{B}}(x) = \exp(\varepsilon^{-1/3}p_0 + p_1 + \varepsilon^{1/3}p_2 + \varepsilon^{2/3}p_3) \tag{19}$$

Equation (19) can be shown to be identical to $y_0^{\mathrm{W}}(x) = \exp(\varepsilon^{-1/2}p_0 + p_1 + \varepsilon^{1/2}p_2)$ obtained using three terms only. Such an outcome persists in other distinguished limits of the form $\varepsilon = \mathcal{O}(S^{-4}, S^{-5}, S^{-6}, S^{-7}, \ldots)$. The only difference among these families of Type III solutions will be the additional penalty requirement of retaining progressively more terms before reaching the same truncation order in ε. The Type III expansion may therefore be deemed a slower converging series of Type I through which no additional benefit may be gained.

IV. On the Composite-Scaling Technique

It is well known that occasions arise for which the traditional method of multiple scales faces intractable obstructions.[35,36] The injection-induced boundary-value problem that has been widely investigated constitutes one such example. In seeking a multiple-scale solution, we find a nonstandard rational analysis to be requisite. This is caused by the need to provide more freedom in the selection of transformations that are capable of handling nonlinear coordinate expansions.

A. Disparity and Nonlinearity

Due to the interactions among diffusive, convective, and inertial mechanisms, our jointly dispersive and dissipative problem exhibits three dissimilar scales. In addition to the outer scale $x_0 = x$, two interior scales have been shown to exist. Near the inner core, the transverse mean flow component vanishes by virtue of $a_0(0) = 0$. The convective cross-flow component, expressed by the first derivative term in Eq. (1), becomes negligible. A balance between diffusive and inertial forces can be then be achieved in Eq. (1) using $x_1 = x_\mathrm{i} = \varepsilon / x^2$. [1,2] The existence of this scale was proved in related work by the author.[4] Near the porous wall, inertial and convective forces dominate, and the use of $x_2 = x_\mathrm{w} = \varepsilon(1-x)$ becomes necessary to achieve a balance in Eq. (1) between the locally dominating mechanisms. In the foregoing, the subscripts 'i' and 'w' refer to the inner-core and near-wall transformations. Note that the nonlinearity in the choice of x_i eludes conventional transformations of the form $x_1 = f(\varepsilon)x$ or $x_1 = f(\varepsilon)(1-x)$. [34,37] In reality, it is the failure of linear transformations that has prompted the search for a more suitable scaling paradigm.

B. Limitation

Due to the disparity and nonlinearity displayed by the scales, a standard three-variable expansion using x_0, x_1 and x_2 leads to a mathematically intractable problem. However, two-variable expansions using only a pair of virtual coordinates (x_0, $x_1 = x_\mathrm{i}$), or (x_0, $x_2 = x_\mathrm{w}$) can produce local approximations that are valid either near the core, or near the wall, respectively. This aspect will be further expounded in Example 3 below. In view of the practical limitation to a two-variable expansion, we have introduced a single composite scale, x_c, that possesses space-reductive properties satisfying

$$x_\mathrm{c} \sim \begin{cases} x_1 = x_\mathrm{i}; & x \to 0 \\ x_2 = x_\mathrm{w}; & x \to 1 \end{cases} \tag{20}$$

If such a function exists, then it can be argued that a two-variable expansion with (x_0, x_c) will, in principle, yield an expression that remains valid uniformly over the solution domain.

C. Matching of the Scales

In the spirit of reproducing x_i and x_w asymptotically near the core and the porous walls, we consider a function that fulfills the requirements stated in Eq. (20), specifically

$$x_\mathrm{c} = \varepsilon(1-x)x^{-2} \tag{21}$$

Proof. Near the core, we let $x = 0 + \Delta x$. The core and composite variables become

$$\begin{cases} x_\mathrm{i} = \varepsilon / \Delta x^2 \\ x_\mathrm{c} = \varepsilon(1-\Delta x) / \Delta x^2 \end{cases} \tag{22}$$

In Eq. (22), it can be seen that $x_\mathrm{c} \sim x_\mathrm{i}$ as $\Delta x \to 0$.

Near the porous wall, we let $x = 1 - \Delta x$. The wall and composite variables become

$$\begin{cases} x_\mathrm{w} = \varepsilon(1-1+\Delta x) = \varepsilon\Delta x \\ x_\mathrm{c} = \varepsilon\Delta x / (1-\Delta x)^2 \end{cases} \tag{23}$$

From Eq. (23), it is clear that $x_\mathrm{c} = \varepsilon\Delta x(1-\Delta x)^{-2} \sim x_\mathrm{w}; \Delta x \to 0$.

We conclude that, since Eq. (21) secures the requirements imposed by Eq. (20), it can be adopted instead of both interior scales to arrive at a uniformly valid, two-variable expansion. This CST expansion must be based on $x_0 = x$ and the *spatially composite variable* $x_1 = x_\mathrm{c}$.

D. Scaling Function

In a two-variable expansion, the second variable can be taken, in general, to be x_i, x_w, or x_c. Depending on the chosen variable, the resulting asymptotic solutions will be accurate near the core, near the wall, or throughout the

domain. To avoid repetition, we find it convenient to define a generally nonlinear scaling function that can, when needed, return any of the following forms

$$x_1 = \varepsilon s(x); \quad \text{where} \qquad s(x) = \begin{cases} s_{\mathrm{i}} = x_{\mathrm{i}} / \varepsilon = 1/x^2; \; s_{\mathrm{w}} = x_{\mathrm{w}} / \varepsilon = (1-x) \\ s_{\mathrm{c}} = x_{\mathrm{c}} / \varepsilon = (1-x)/x^2; \; s_{\mathrm{g}} \end{cases} \tag{24}$$

Here, s_{g} corresponds to a general scaling function that remains, at present, unspecified; s_{i}, s_{w}, s_{c} retain their usual significance.

E. Two-Variable Expansions

Using $x_0 = x$ and $x_1 = \varepsilon s(x)$, derivatives become

$$\frac{\mathrm{d}}{\mathrm{d}x} = \frac{\partial}{\partial x_0} + \varepsilon s' \frac{\partial}{\partial x_1}, \quad \frac{\mathrm{d}^2}{\mathrm{d}x^2} = \frac{\partial^2}{\partial x_0^2} + \mathcal{O}(\varepsilon) \tag{25}$$

Substitution into Eq. (1) gives

$$\varepsilon \frac{\partial^2 y}{\partial x_0^2} + \left(a_0 + \varepsilon a_1\right) \frac{\partial y}{\partial x_0} + a_0 \varepsilon s' \frac{\partial y}{\partial x_1} + \left(b_0 + iSc_0\right) y + \varepsilon b_1 y + \mathcal{O}(\varepsilon^2) = 0 \tag{26}$$

Next, we insert $y = y_0 + \varepsilon y_1 + \mathcal{O}(\varepsilon^2)$ into Eq. (26) and combine terms of the same order in ε. At $\mathcal{O}(1)$, the leading-order equation may be taken as

$$a_0 \frac{\partial y_0}{\partial x_0} + \left(b_0 + iSc_0\right) y_0 = 0 \tag{27}$$

Subsequent integration in x_0 yields

$$y_0(x_0, x_1) = C_1(x_1) e^{w}, \qquad w(x_0) \equiv -\int^{x_0} (b_0 + iSc_0) / a_0 \mathrm{d}t \tag{28}$$

In like fashion, the first-order equation becomes

$$a_0 \frac{\partial y_1}{\partial x_0} + \left(b_0 + iSc_0\right) y_1 = -a_0 s' \frac{\partial y_0}{\partial x_1} - a_1 \frac{\partial y_0}{\partial x_0} - b_1 y_0 - \frac{\partial^2 y_0}{\partial x_0^2} \tag{29}$$

F. Solvability Condition

In seeking y_1, the adjointness concept may be employed. This is accomplished by setting $y_1 = y_0 g(x_0)$. In order to determine g, one multiplies Eq. (27) by $a_0^{-1} y_1 y_0^{-2}$ and subtracts the product from Eq. (29) times $a_0^{-1} y_0^{-1}$. Two terms cancel with the remainder being

$$\frac{\partial g}{\partial x_0} = \frac{1}{y_0} \frac{\partial y_1}{\partial x_0} - \frac{y_1}{y_0^2} \frac{\partial y_0}{\partial x_0} = -\frac{s'}{y_0} \frac{\partial y_0}{\partial x_1} - \frac{1}{a_0 y_0} \frac{\partial^2 y_0}{\partial x_0^2} - \frac{a_1}{a_0 y_0} \frac{\partial y_0}{\partial x_0} - \frac{b_1}{a_0} \tag{30}$$

By virtue of the principle of least singular behavior, the ratio of y_1 and y_0 must be remain perpetually bounded to ensure a series of successively decreasing terms. This can be achieved by imposing

$$g(x_0) = -\int^{x_0} \left(\frac{s'}{y_0} \frac{\partial y_0}{\partial x_1} + \frac{1}{a_0 y_0} \frac{\partial^2 y_0}{\partial x_0^2} + \frac{a_1}{a_0 y_0} \frac{\partial y_0}{\partial x_0} + \frac{b_1}{a_0} \right) \mathrm{d}t = \mathcal{O}(1) \tag{31}$$

From Eq. (28), derivatives may be evaluated straightforwardly. One finds

$$g(x_0) = -\int^{x_0} \left[\frac{s'(t)}{C_1(x_1)} \frac{\mathrm{d}C_1(x_1)}{\mathrm{d}x_1} + \frac{w''(t) + w'^2(t) + a_1 w'(t) + b_1(t)}{a_0(t)} \right] \mathrm{d}t = \mathcal{O}(1) \tag{32}$$

G. Imposing a Sufficient Condition

Irrespective of how large x_0 may be, a sufficient condition that ensures the boundedness of g may be obtained by setting

$$\frac{s'}{C_1(x_1)} \frac{\mathrm{d}C_1(x_1)}{\mathrm{d}x_1} + \frac{w'' + w'^2 + a_1 w' + b_1}{a_0} = 0 \tag{33}$$

Subsequent integration with respect to x_1 renders

$$C_1 = C_0 \exp\left[-(w'' + w'^2 + a_1 w' + b_1) x_1 / (a_0 s') \right] \tag{34}$$

In the above, C_0 is a pure constant that may be determined from the boundary condition at $x=1$ in Eq. (2). Returning to the original laboratory coordinate x, the multiple-scale solution to the first order in ε can be put in the form

$$y^{\mathrm{C}}(x)=\exp\Big\{w(x)-w(1)+\varepsilon\eta(x)\Big[w''(x)+w'^2(x)+a_1(x)w'(x)+b_1(x)\Big]/a_0(x)$$
$$-\varepsilon\eta(1)\Big[w''(1)+w'^2(1)+a_1(1)w'(1)+b_1(1)\Big]/a_0(1)\Big\}+\mathcal{O}(\varepsilon);\qquad \eta(x)\equiv -s(x)/s'(x) \tag{35}$$

and

$$w'=-(b_0+iSc_0)/a_0,\qquad w''+w'^2=[(-S^2c_0^2+b_0^2+a_0'b_0-a_0b_0')+iS(a_0'c_0-a_0c_0'+2b_0c_0)]/a_0^2 \tag{36}$$

where the superscript 'C' refers to an approximation based on the 'CST' approach. Backward substitution of the variable coefficients renders:

$$y^{\mathrm{C}}(x)=\exp\Big\{w(x)-w(1)+\varepsilon\eta(x)a_0^{-3}\Big[-S^2c_0^2+b_0^2+a_0'b_0-a_0b_0'-a_0a_1b_0+a_0^2b_1+iS(a_0'c_0-a_0c_0'+2b_0c_0-a_0a_1c_0)\Big]$$
$$-\varepsilon\eta(1)a_0^{-3}(1)\Big[-S^2c_0^2+b_0^2+a_0'b_0-a_0b_0'-a_0a_1b_0+a_0^2b_1+iS(a_0'c_0-a_0c_0'+2b_0c_0-a_0a_1c_0)\Big]_{x=1}\Big\}+\mathcal{O}(\varepsilon) \tag{37}$$

The resulting expression may be rearranged to the extent of extracting the group parameter εS^2. We get

$$y^{\mathrm{C}}(x)=\exp\Big(w(x)-w(1)-\eta a_0^{-3}\Big\{\varepsilon S^2\Big[c_0^2-S^{-2}\Big(b_0^2+a_0'b_0-a_0b_0'-a_0a_1b_0+a_0^2b_1\Big)\Big]+i\varepsilon S\Big(a_0c_0'-a_0'c_0+a_0a_1c_0-2b_0c_0\Big)\Big\}$$
$$+\eta(1)a_0^{-3}(1)\Big\{\varepsilon S^2\Big[c_0^2-S^{-2}\Big(b_0^2+a_0'b_0-a_0b_0'-a_0a_1b_0+a_0^2b_1\Big)\Big]+i\varepsilon S\Big(a_0c_0'-a_0'c_0+a_0a_1c_0-2b_0c_0\Big)\Big\}_{x=1}\Big)+\mathcal{O}(\varepsilon) \tag{38}$$

The real part of the wave solution can, in turn, be expressed as

$$\Re\Big[y^{\mathrm{C}}(x)\Big]=\exp\Bigg(-\Big\{\varepsilon S^2\eta a_0^{-3}\Big[c_0^2-S^{-2}\Big(b_0^2+a_0'b_0-a_0b_0'-a_0a_1b_0+a_0^2b_1\Big)\Big]-w\Big\}_1^x\Bigg)$$
$$\times\cos\Big\{\varepsilon S\Big[\eta a_0^{-3}\Big(a_0c_0'-a_0'c_0+a_0a_1c_0-2b_0c_0\Big)\Big]_1^x\Big\}+\mathcal{O}(\varepsilon) \tag{39}$$

H. Avoidance of Singularity

At this stage, it may be instructive to note that the amplitude of the CST solution is prescribed by the dominant term that controls the wave's exponential growth or decay. To avoid unboundedness, say at $x=0$, the sign of the most dominant term cannot be permitted to trigger exponential growth. Given the multiply-perturbed nature at hand, situations may be conceived for which a singularity will occur unless the small contribution of $\mathcal{O}(S^{-2})$ is suppressed in Eq. (39). Dismissal of the quantity in question may be justified when the parametric excursions over which ε varies remain of $\mathcal{O}(S^{-1})$ or smaller, such as $\mathcal{O}(S^{-2})$. Under these auspices, the $\mathcal{O}(S^{-2})$ component of Eq. (39) may be absorbed by the truncation error, thus leading to a compact expression for the CST approximation,

$$\hat{y}^{\mathrm{C}}(x)=\exp\Big\{w(x)-w(1)-\varepsilon S^2\Big[\eta(x)a_0^{-3}(x)c_0^2(x)-\eta(1)a_0^{-3}(1)c_0^2(1)\Big]$$
$$-i\varepsilon S\Big[\eta a_0^{-3}\Big(a_0c_0'-a_0'c_0+a_0a_1c_0-2b_0c_0\Big)\Big]_1^x\Big\}+\mathcal{O}(\varepsilon) \tag{40}$$

where $\hat{y}^{\mathrm{C}}$ is always bounded. It can be shown that such an expression will be less prone to singularities,[38] although the added robustness is usually accompanied by a slight reduction in precision with respect to Eq. (38). In the forthcoming analysis, the full expression will be employed, barring situations that warrant the dismissal of the higher order quantities that naturally crop up in the CST expansion. The issue of boundedness will also be addressed in the concrete examples ahead.

I. Local and Composite Length Scales

In Eq. (35), $\eta(x)$ lingers as the only unspecified quantity that needs to be defined. Physically, $\eta(x)$ can represent the characteristic length scale for normal or radial wave convection away from the porous walls. Based on Eq. (24), one finds

$$\eta(x)=\begin{cases}\eta_{\mathrm{i}}=x/2;\ \eta_{\mathrm{w}}=(1-x)\\ \eta_{\mathrm{c}}=x(x-1)/(x-2)\end{cases} \tag{41}$$

When η_i, η_w and η_c are each substituted back into Eq. (35), three different solutions y^i, y^w and y^C are realized. With y^N denoting the numerical solution of the governing equation, then it can be verified that y^i, y^w and y^C will be reasonable approximations to y^N in the near-core region, near-wall region, and uniformly throughout the domain, respectively. The degree of accuracy in these approximations will stay, of course, commensurate with the size of ε. These remarks will be clarified in the Example 3 below.

V. On the Generalized-Scaling Technique

In order to determine y^C, the form of s_c and corresponding η_c have to be known. This pre-selection of the modified scaling transformation is consistent with standard multiple-scale practices. At the expense of presetting the scales, however, the need arises to use a stronger constraint than is required by our problem's solvability condition. A sufficient albeit unnecessary condition is therefore used in Eq. (33) to secure a uniformly valid outcome. For instance, although Eq. (33) satisfies the solvability condition, it may not always lead to a rational approximation. On that account, it may be argued that a more rigorous approach must offer the freedom to employ a coordinate transformation that fully complies with the requirements needed for solvability. This notion is explored next.

A. A Necessary and Sufficient Condition

Equation (32) can be rewritten as

$$g(x_0) = -\frac{s(x_0)}{C_1(x_1)}\frac{\mathrm{d}C_1(x_1)}{\mathrm{d}x_1} - \int^{x_0}\left[\frac{w''(t)+w'^2(t)+a_1w'(t)+b_1(t)}{a_0(t)}\right]\mathrm{d}t = \mathcal{O}(1) \tag{42}$$

In order for the function g to be bounded for arbitrary variable coefficients, $\forall x_1$, and $x_0 = \mathcal{O}(\varepsilon^{-1})$, it is necessary and sufficient that

$$\frac{1}{C_1(x_1)}\frac{\mathrm{d}C_1(x_1)}{\mathrm{d}x_1} = \mu \qquad \Rightarrow C_1(x_1) = C_0\exp(\mu x_1) \tag{43}$$

where μ is a subsidiary constant. Inserting Eq. (43) back into Eq. (42) yields a formal expression for $s(x)$. This is

$$s(x_0) = -\mu^{-1}\int^{x_0}\left[\frac{w''(t)+w'^2(t)+a_1w'(t)+b_1(t)}{a_0(t)}\right]\mathrm{d}t - \mu^{-1}g(x_0) \tag{44}$$

In the above, $g(x)$ can be any bounded function. The generality of form assigned to $s(x)$ makes satisfying Eq. (44) possible.

B. Generalized Solution

Recalling that $x_1 = \varepsilon s$, we now return to the original variable x and substitute Eq. (44) back into Eqs. (43) and (28). In the process, μ is fully eliminated! The resulting expression reads

$$y_0(x) = C_0\exp\left[w(x) - \varepsilon\int^x a_0^{-1}\left(w'' + w'^2 + a_1w' + b_1\right)\mathrm{d}t - \varepsilon g(x)\right] \tag{45}$$

By insisting on $g(x) = \mathcal{O}(1)$ for boundedness, it follows that $\exp(-\varepsilon g) = 1 + \mathcal{O}(\varepsilon)$. As such, g does not influence the solution that we seek at $\mathcal{O}(\varepsilon)$. It can be safely dismissed hereafter. The remaining constant C_0 can be evaluated from the boundary condition at $x = 1$. At length, using 'G' for 'general,' we write

$$y^G(x) = \exp\left\{w(x) - w(1) - \varepsilon\int_1^x a_0^{-1}\left(w'' + w'^2 + a_1w' + b_1\right)\mathrm{d}t\right\} + \mathcal{O}(\varepsilon) \tag{46}$$

where $a_0^{-1}\left(w'' + w'^2 + a_1w' + b_1\right)$

$$= [(-S^2c_0^2 + b_0^2 + a_0'b_0 - a_0b_0' - a_0a_1b_0 + a_0^2b_1) + iS(a_0'c_0 - a_0c_0' + 2b_0c_0 - a_0a_1c_0)]/a_0^3 \tag{47}$$

By inspection of Eqs. (35) and (46) the term multiplying $-S^2c_0^2/a_0^3$ appears to be the largest. It thus dictates the exponential rate of decay of the wave amplitude. This is evident in the result obtained by substituting Eq. (47) back into Eq. (46). The outcome is:

$$y^G(x) = \exp\left\{w(x) - w(1) + \varepsilon S^2\int_1^x a_0^{-3}\left[c_0^2 - S^{-2}(b_0^2 + a_0'b_0 - a_0b_0' - a_0a_1b_0 + a_0^2b_1)\right.\right.$$
$$\left.\left. + iS^{-1}(a_0c_0' - a_0'c_0 - 2b_0c_0 + a_0a_1c_0)\right]\mathrm{d}t\right\} + \mathcal{O}(\varepsilon) \tag{48}$$

When compared to y^W in Eq. (13), y^G shares, at leading order, the same exponential arguments. However, y^G contains additional correction terms in its real part that are of $\mathcal{O}(S^{-2})$. These are accompanied by slightly improved

accuracy which may be attributed, in part, to the use of information belonging to the first-order equation in y_1 during the leading-order evaluation of C_1 in Eq. (28). Such quantities in the comparable WKB solution of Type I emerge at the next perturbative order (i.e., in y_1^{W} instead of y_0^{W}). The reader is cautioned, however, that the added precision is not gained without penalty. It may be shown for some cases that the retention of $\mathcal{O}(S^{-2})$ terms in Eq. (48) can make the solution vulnerable to singularities. Here too, the amplitude of y^{G} will be governed by the coefficient of the most singular term in the exponential. For some values of the control parameters, boundedness will be contingent on securing the (negative) sign of the most dominant term. Then given the small size of the $\mathcal{O}(S^{-2})$ contribution, it can be systematically lumped with the truncation order to the extent of producing a bounded solution independently of the control parameters. This expression may be written as

$$\hat{y}^{\mathrm{G}}(x) = \exp\left\{w(x) - w(1) + \varepsilon S^2 \int_1^x a_0^{-3}\left[c_0^2 + iS^{-1}(a_0 c_0' - a_0' c_0 - 2b_0 c_0 + a_0 a_1 c_0)\right]\mathrm{d}t\right\} + \mathcal{O}(\varepsilon) \tag{49}$$

Interestingly, this compact and robust form differs from the comparable Type I WKB expansion by one member only. When benchmarked to Eq. (49), $y_0^{\mathrm{W}}(x)$ is seen to comprise one additional imaginary term that affects its phase angle. One finds

$$\frac{y^{\mathrm{W}}(x)}{\hat{y}^{\mathrm{G}}(x)} = \exp\left\{2i\varepsilon^2 S^3 \int_1^x c_0^3 a_0^{-5}\mathrm{d}t\right\} \tag{50}$$

The contribution of this term is typically small, albeit more difficult to evaluate in view of its dependence on the integrability of $c_0^3 a_0^{-5}$.

C. Deducing the Generalized-Scaling Function

Since traditional approaches require guessing the inner scaling transformation before expanding the derivatives, we find it expedient to define s_{g} to be the general inner transformation that can lead to Eq. (46) in a conventional multiple-scale expansion. With no loss of generality, it can be seen from Eqs. (46), (43) and (28) that the effective scale provided by the solvability condition is

$$s_{\mathrm{g}}(x) \propto \int^x a_0^{-1}\left(w'' + w'^2 + a_1 w' + b_1\right)\mathrm{d}t \tag{51}$$

Based on Eq. (35), the characteristic length scale stemming from the generalized formulation becomes

$$\eta_{\mathrm{g}}(x) = -\frac{s_{\mathrm{g}}(x)}{s_{\mathrm{g}}'(x)} = -\frac{\int^x a_0^{-1}\left(w'' + w'^2 + a_1 w' + b_1\right)\mathrm{d}t}{a_0^{-1}\left(w'' + w'^2 + a_1 w' + b_1\right)} \tag{52}$$

This expression is different from the composite η_{c} given in Eq. (41). Unlike the previous result that was obtained from initial guesswork, the present solution is prescribed at the conclusion of the asymptotic analysis. It is established in a manner to fully comply with the problem's solvability condition.

Clearly, the GST scheme just described is capable of capturing the dominant behavior of the problem at hand. However, it represents a subset of an even more general approach in which the generalized scale is granted more freedom by being expanded in series form. For problems that exhibit a different character or in which several successive corrections are desired, a broader formulation is required. In this case, the general scale in Eq. (24) may be expanded as

$$x_1 = \delta^{-1}x_0 + x_1 + \delta x_2 + \delta^2 x_3 + \delta^3 x_4 + \ldots \tag{53}$$

This particular series expansion of the generalized scale is analogous to the argument of Eq. (3). When applied in concert with multiple-scale theory, it has the potential to restore the WKB solutions described above. Yet given the level of detail prescribed by the attendant analysis, it will be the subject of a forthcoming study.

VI. Example 1: Wave Propagation in Cylindrical Cavity

In order to set a rigorous benchmark for comparisons, we explore a case for which Eq. (1) comprises $a_0 = x$, $a_1 = 1/x$, $b_0 = -2\lambda = -4(n+1), n = 0,1,\ldots$, $b_1 = 0$ and $c_0 = 1$. The boundary-layer equation becomes

$$\varepsilon y'' + \left(x + \varepsilon/x\right)y' + \left(-2\lambda + iS\right)y = 0; \qquad y'(0) = 0, \qquad y(1) = 1. \tag{54}$$

We propose to solve Eq. (54) both exactly and asymptotically. The pertinent physical problem is analogous to that described for the vortical wave propagation equation of motion in rectangular channels with porous walls.[4,5] The present model corresponds to porous tubes with circular cross sections. As such, two dissimilar scales, $x_0 = x$ and $x_1 = x_{\mathrm{i}}$, may be anticipated.

A. Whittaker Equation

An exact solution is feasible through a series of manipulations guided by the Liouville-Green procedure. After some algebra, we recognize the need for the dual transformations,

$$X = x^2/(2\varepsilon) \qquad F(X) = \sqrt{X}\exp(\tfrac{1}{2}X)y(x) = (x/\sqrt{2\varepsilon})\exp\left[x^2/(4\varepsilon)\right]y(x) \tag{55}$$

By setting these preferences, backward substitution changes Eq. (54) into the Whittaker equation,

$$\frac{\mathrm{d}^2F}{\mathrm{d}X^2} + \left[-\tfrac{1}{4} + \frac{\kappa}{X} + \left(\tfrac{1}{4}-0\right)\frac{1}{X^2}\right]F = 0; \qquad \kappa \equiv \tfrac{1}{2}iS - \lambda - \tfrac{1}{2} \tag{56}$$

Interestingly, the general solution for Eq. (56) is expressible in terms of Φ and U, the Kummer and regular confluent hypergeometric functions.[39] These give

$$y(x) = \exp(-\tfrac{1}{2}x^2/\varepsilon)\left[C_1\Phi\left(1+\lambda-\tfrac{1}{2}iS,1,\tfrac{1}{2}x^2/\varepsilon\right) + C_2U\left(1+\lambda-\tfrac{1}{2}iS,1,\tfrac{1}{2}x^2/\varepsilon\right)\right] \tag{57}$$

B. Exact Solution

At present, the $y'(0)=0$ requirement proves to be redundant; it is unconditionally satisfied by Eq. (57) irrespective of C_1 and C_2. The physical existence condition at $x=0$ must be used instead. Thus, in order to ensure that the solution is finite at the core, C_2 must vanish. The remaining constraint at $x=1$ yields C_1. Then using the superscript E for 'exact,' we can put

$$y^{\mathrm{E}}(x) = \exp\left[\tfrac{1}{2}\varepsilon^{-1}(1-x^2)\right]\Phi\left(\nu,1,\tfrac{1}{2}\varepsilon^{-1}x^2\right)/\Phi\left(\nu,1,\tfrac{1}{2}\varepsilon^{-1}\right), \quad \nu \equiv 1+\lambda-\tfrac{1}{2}iS \tag{58}$$

where

$$\Phi(\nu,1;x) = 1 + \nu\frac{x}{(1!)^2} + \nu(\nu+1)\frac{x^2}{(2!)^2} + \nu(\nu+1)(\nu+2)\frac{x^3}{(3!)^2} + \ldots \tag{59}$$

We note, in passing, that the inner-core scale $x_{\mathrm{i}} = \varepsilon x^{-2}$ appears explicitly in y^{E}, albeit inverted.

C. WKB Solution

Using Eq. (13), the Type I solution can be explicitly evaluated. We get

$$y^{\mathrm{W}} = y_0^{\mathrm{W}} = x^{2\lambda}\exp\left\{-\tfrac{1}{2}\xi(x^{-2}-1) - iS\left[\ln x + \tfrac{1}{2}\varepsilon(x^{-2}-1)(\xi+4\lambda+\xi x^{-2})\right]\right\} + \mathcal{O}(\varepsilon) \tag{60}$$

Higher-order solutions can be constructed as well. These result in

$$\begin{aligned} y_1^{\mathrm{W}} = x^{2\lambda}\exp\Big(&-\tfrac{1}{2}\xi(x^{-2}-1)\Big\{1 + S^{-2}\left[2\lambda(1-2\lambda) + \tfrac{3}{2}\xi(1+x^{-2})(4\lambda-1) + \tfrac{5}{3}\xi^2(1+x^{-2}+x^{-4})\right]\Big\} \\ &-iS\Big\{\ln x + \tfrac{1}{2}\varepsilon(x^{-2}-1)(\xi+4\lambda+\xi x^{-2}) - \tfrac{1}{2}\varepsilon^2(x^{-2}-1)\Big[6\lambda(2\lambda-1)(1+x^{-2}) \\ &+\tfrac{2}{3}\xi(20\lambda-7)(1+x^{-2}+x^{-4}) + \tfrac{7}{2}\xi^2(1+x^{-2})(1+x^{-4})\Big]\Big\}\Big) + \mathcal{O}(\varepsilon^2) \end{aligned} \tag{61}$$

$$\begin{aligned} y_2^{\mathrm{W}} = x^{2\lambda}\exp\Big[&-\tfrac{1}{2}\xi(x^{-2}-1)\Big(1 + S^{-2}\Big\{2\lambda(1-2\lambda) + \tfrac{3}{2}\xi(1+x^{-2})(4\lambda-1) + \tfrac{5}{3}\xi^2(1+x^{-2}+x^{-4}) + \varepsilon(1+x^{-2}) \\ &\times\Big[2\lambda(1-2\lambda)^2 + \xi^2(35\lambda-16)(1+x^{-4})\Big] + 4\varepsilon\xi(1+x^{-2}+x^{-4})(1-\tfrac{22}{3}\lambda+10\lambda^2) + \tfrac{42}{5}\varepsilon\xi^3(1-x^{-10})/(1-x^{-2})\Big\}\Big) \\ &-iS\Big(\ln x + \tfrac{1}{2}\varepsilon(x^{-2}-1)\Big\{(\xi+4\lambda+\xi x^{-2}) - \varepsilon\Big[6\lambda(2\lambda-1)(1+x^{-2}) + \tfrac{7}{2}\xi^2(1+x^{-2})(1+x^{-4}) + \tfrac{2}{3}\xi(20\lambda-7) \\ &\times(1+x^{-2}+x^{-4})\Big] + \varepsilon^2\Big[\tfrac{8}{3}\lambda(7-24\lambda+20\lambda^2)(1+x^{-2}+x^{-4}) + \xi(21-132\lambda+140\lambda^2)(1+x^{-2})(1+x^{-4}) \\ &+\tfrac{56}{3}\xi^2(9\lambda-5)(1-x^{-10})/(1-x^{-2}) + 22\xi^3(1+x^{-2}+x^{-4})(1+x^{-6})\Big]\Big\}\Big)\Big] + \mathcal{O}(\varepsilon^3) \end{aligned} \tag{62}$$

Using Eqs. (16)-(17), the Type II solution can be determined as well. After some algebra, one finds

$$\begin{aligned} y^{\mathrm{K}} = x^{2\lambda}&\left(\frac{1+16\varepsilon^2S^2}{1+16\varepsilon^2S^2x^{-4}}\right)^{\frac{1}{8}}\left(\frac{1+\sqrt{1-4i\varepsilon Sx^{-2}}}{1+\sqrt{1-4i\varepsilon S}}\right)^{1+2\lambda}\exp\left(-\frac{x^2}{4\varepsilon}\left[1-\sqrt{1-4i\varepsilon Sx^{-2}} + x^{-2}\left(-1+\sqrt{1-4i\varepsilon S}\right)\right]\right. \\ &\left.-iS\left\{\ln x + \ln\left(\frac{1+\sqrt{1-4i\varepsilon Sx^{-2}}}{1+\sqrt{1-4i\varepsilon S}}\right) + \frac{1}{4S}\tan^{-1}\left[\frac{4\varepsilon S(1-x^{-2})}{1+16\varepsilon^2S^2x^{-2}}\right]\right\}\right) + \mathcal{O}(\varepsilon) \end{aligned} \tag{63}$$

It is interesting to note that, in both y^{W} and y^{K}, the $x^{2\lambda}$ term forces the traveling wave amplitude to decay more rapidly as $\lambda \to \infty$.

D. Traditional Multiple-Scale Expansion

In applying the conventional derivative-expansion procedure, it may be helpful to remark that the solution must be similar to its equivalent arising in a rectangular geometry. The latter was described by Majdalani[4,5] where it was obtained using $x_0 = x$ and $x_1 = \varepsilon x^{-2}$. Using the same two scales as before and letting $y = y_0 + \varepsilon y_1 + \mathcal{O}(\varepsilon^2)$, derivatives can be expanded and substituted into Eq. (54). Collecting terms of $\mathcal{O}(\varepsilon^0)$ and $\mathcal{O}(\varepsilon^1)$, one segregates

$$\varepsilon^0: \quad x\frac{\partial y_0}{\partial x_0} + \left(-2\lambda + iS\right) y_0 = 0 \tag{64}$$

$$\varepsilon: \quad x\frac{\partial y_1}{\partial x_0} + \left(-2\lambda + iS\right) y_1 = 2x^{-2}\frac{\partial y_0}{\partial x_1} - x^{-1}\frac{\partial y_0}{\partial x_0} - \frac{\partial^2 y_0}{\partial x_0^2} \tag{65}$$

Partial integration of Eq. (64) yields

$$y_0(x_0, x_1) = C_1(x_1)\exp\left[(2\lambda - iS)\ln x_0\right] \tag{66}$$

Following the solvability condition given in Eq. (31), we now have

$$\frac{\mathrm{d}C_1}{\mathrm{d}x_1} - \tfrac{1}{2}\left[-S^2 + 4\lambda(\lambda - iS)\right]C_1 = 0 \text{ or } C_1(x_1) = C_0 \exp\left\{\tfrac{1}{2}\left[-S^2 + 4\lambda(\lambda - iS)\right]x_1\right\} \tag{67}$$

Recalling that $x_1 = \varepsilon x^{-2}$, Eq. (66) becomes

$$y_0(x) = C_0 \exp\left\{(2\lambda - iS)\ln x + \tfrac{1}{2}\varepsilon x^{-2}\left[-S^2 + 4\lambda(\lambda - iS)\right]\right\} \tag{68}$$

Then using the boundary condition at $x = 1$, the traditional multiple-scale solution collapses into

$$y^{\mathrm{T}}(x) = x^{2\lambda}\exp\left\{-\tfrac{1}{2}(\xi - 4\varepsilon\lambda^2)(x^{-2} - 1) - iS\left[\ln x + 2\varepsilon\lambda(x^{-2} - 1)\right]\right\} + \mathcal{O}(\varepsilon) \tag{69}$$

where the superscript 'T' stands for 'traditional.' Due to the multiply-perturbed nature of this problem, the absence of singularity in Eq. (69) at $x = 0$ depends on the physical ranges over which the dominant coefficient $\xi - 4\varepsilon\lambda^2 \geq 0$. This condition translates into $\varepsilon S^2 \geq 4\varepsilon\lambda^2$ or $S \geq 2|\lambda|$. Conversely, when the $4\varepsilon\lambda^2$ contribution to the exponential argument in y^{T} is dismissed, unboundedness is uniformly suppressed. Equation (69) becomes

$$\tilde{y}^{\mathrm{T}}(x) = x^{2\lambda}\exp\left\{-\tfrac{1}{2}\xi(x^{-2} - 1) - iS\left[\ln x + 2\varepsilon\lambda(x^{-2} - 1)\right]\right\} + \mathcal{O}(\varepsilon) \tag{70}$$

In what follows, we assume that $S \geq 2|\lambda|$ to the extent of warranting the use of Eq. (69).

E. CST Solution

Alternatively, in the presence of a single inner (nonlinear) variable, $x_1 = x_{\mathrm{i}} = \varepsilon x^{-2}$, the composite scale may be used to identically reproduce the inner coordinate transformation. Letting $s_{\mathrm{c}} = s_{\mathrm{i}}$, one can legitimately derive and use $\eta_{\mathrm{c}} = \eta_{\mathrm{i}} = -x_1 / x_1' = x/2$ in the CST approximation. At the outset, Eq. (35) becomes

$$y^{\mathrm{C}} = x^{2\lambda}\exp\left\{-\xi(1 + 2i\lambda/S)^2\left[\eta(x)/x^3 - \eta(1)\right] - iS\ln x\right\} + \mathcal{O}(\varepsilon); \quad \eta = x/2 \tag{71}$$

Upon expansion and rearrangement, it may be readily shown that Eq. (69) may be restored, term-by-term, from Eq. (71). This confirms the legitimacy of the CST procedure for this particular ODE.

F. GST Solution

In the preceding multiple-scale analyses, identification of the inner scale was necessary. Either foreknowledge or guesswork preceded the selection of the correct inner transformation. This procedural burden, which is only exacerbated in the presence of nonlinear scaling distortions, is mitigated with the use of the generalized-scaling function. For example, using Eq. (51), one may evaluate

$$\int^x a_0^{-1}\left(w'' + w'^2 + a_1 w' + b_1\right)\mathrm{d}t = \left[\tfrac{1}{2}S^2 - 2\lambda(\lambda - iS)\right]x^{-2} + \text{const} \tag{72}$$

This step readily displays $s_{\mathrm{g}}(x) = \mathcal{O}(x^{-2})$ with no need for guesswork. Furthermore, regardless of whether s_{g} is explicitly determined or not, the GST solution may be constructed directly from Eq. (48). Starting with

$$y^{\mathrm{G}}(x) = \exp\left\{(2\lambda - iS)\ln x - \varepsilon\int_1^x\left[-S^2 + 4\lambda(\lambda - iS)\right]x^{-3}\mathrm{d}t\right\} + \mathcal{O}(\varepsilon) \tag{73}$$

it may be promptly shown that y^{G} is identical to both y^{T} and y^{C} for the case at hand.

In summary, a total of five asymptotic schemes have been successfully applied to Eq. (54). Of the five, the three solutions based on multiple scales are found to be identical. Despite its complexity, y^{K} appears to be the most

accurate when ε is relatively large. Among y^{W}, y^{K} and $y^{\mathrm{G}}(=y^{\mathrm{T}}=y^{\mathrm{C}})$, y^{G} appears to be the most accurate and straightforward as $\varepsilon \to 0$, at least in the ranges explored. This behavior will be illustrated next.

G. Exact vs. Asymptotic Solutions

By inspection of the real and imaginary arguments in Eqs. (60) and (69), one can infer that the solution is of the damped oscillatory type. This character is ascertained in Fig. 1 where exact and asymptotic solutions of $\mathcal{O}(\varepsilon)$ are compared at select values of the control parameters. For fixed $\varepsilon = 10^{-2}$, the agreement between y^{W} and y^{E} in Fig. 1a deteriorates progressively in Figs. 1b and 1c. This adverse trend can be attributed to increasing S beyond the $\sqrt{R} = 10$ value for which the Type I WKB expansion is optimized in Fig. 1a. In fact, for the physical settings associated with Figs. 1a-c, it is clear that a quick damping response is taking place. Thus, in all three subfigures, the Type II solution becomes a more suitable approximation. When the primary parameter is decreased to $\varepsilon = 10^{-3}$ in Fig. 1d, the agreement improves to the point that asymptotics become graphically indiscernible from y^{E}.

H. Error Comparison

To more effectively measure the level of agreement entailed in each method, we compare the maximum discrepancy in each formulation with reference to the exact solution y^{E}. We thus turn our attention to the maximum absolute error E that exists between a given asymptotic y^{ε} and exact y^{E}. Defining $E = \max\left|y^{\varepsilon} - y^{\mathrm{E}}\right|$, we then plot E versus ε at fixed values of S and λ. As shown in Fig. 2, a log-log plot can help to characterize the error through variations in λ, S and ε. Assuming the classic logarithmic form, $E = K\varepsilon^{m}$, the order of the error m can be either inferred directly from the graph or calculated numerically using linear least-squares. Whereas m corresponds to the slope, K is deducible from the vertical intercept. As a result, we find in Fig. 2a that the multiple-scale solution exhibits an error of order $m \to 2$ as $\varepsilon \to 0$. Furthermore, the coefficient K and, in turn, the maximum error, diminish as λ increases or S decreases. The accelerated convergence rate in the leading-order y^{G} represents an added benefit. In principle, it can be ascribed to the usage of a solvability condition that taps artificially into the second-order equation.

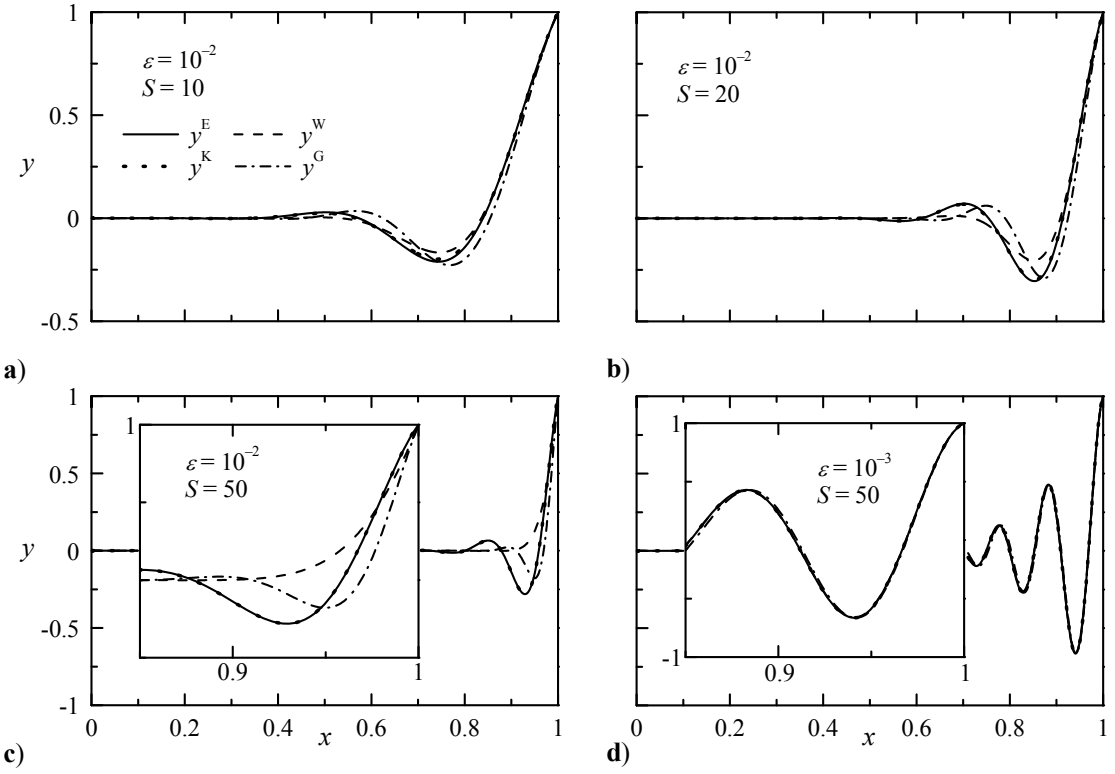

Figure 1. Comparison between y^{E} (exact) and y^{W} (WKB Type I), y^{K} (WKB Type II), and $y^{\mathrm{G}} = y^{\mathrm{C}} = y^{\mathrm{T}}$ (GST, CST, and traditional multiple-scale solutions). For $\varepsilon = 10^{-2}$ and $\lambda = 2$, S is varied from a) 10, to b) 20 and c) 50. Results become indiscernible in d) where ε is decreased by one order while keeping $S = 50$. Insets are used for enlargements.

The trends in the WKB solution of $\mathcal{O}(\varepsilon)$ are somewhat reversed. As depicted in Fig. 2b, the error in y^{W} starts at $m \approx 2$ and then shifts to $m = 1$ asymptotically in ε. Furthermore, both K and E increase as λ or S increase. According to Bosley,[40] the shift in the slope from 2 to 1 does not undermine the validity of the WKB solution because its error exhibits a clear asymptotic order over finite ranges of ε.

The error in y^{K}, on the other hand, behaves quite differently. It fluctuates for $\varepsilon < 10^{-3}$ before shifting to $m = 1$. Whereas both K and E increase as λ increases, the error in y^{K} keeps diminishing with further increases in S. This behavior favors y^{K} for relatively large ε and S when it clearly outperforms its various counterparts. However, unlike y^{G}, both y^{W} and y^{K} become relatively less accurate at higher values of λ (or n).

The WKB solution of $\mathcal{O}(\varepsilon^3)$ is defined in Eq. (62) and shown in Fig. 2c. Despite this high of an order, its error exhibits $m \approx 3$ over a range of ε. However, this order shifts to $m \approx 1$ as ε is decreased. Here, the error appears to

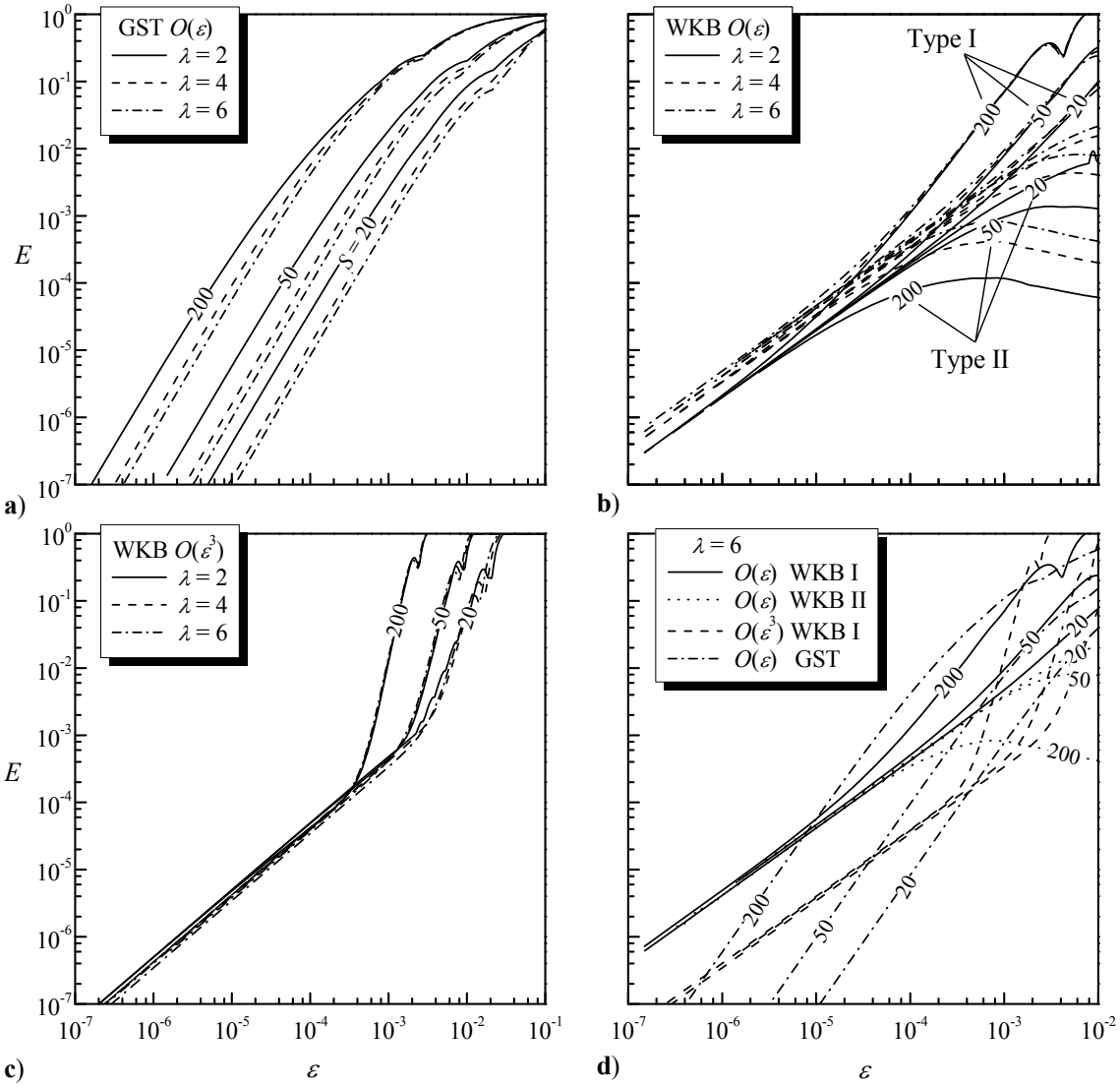

Figure 2. Log-log plot of the absolute error versus ε at constant S. The error in $y_0^{\mathrm{C}} = y_0^{\mathrm{G}}$ is shown in a) for $\lambda = 2,4$ and 6. Unlike a), the error in the WKB solution does not decrease at higher integers. This is illustrated in both b) and c) where y_0^{W}, y_0^{K} (WKB Types I and II) and y_2^{W} are analyzed. Note that the $\mathcal{O}(\varepsilon^3)$ WKB solution in c) starts with an error of order 3 and then shifts to 1 as $\varepsilon \to 0$. When errors are compared in d) for $\lambda = 6$ and $S = 20,50$ and 200, the $\mathcal{O}(\varepsilon)$ multiple-scale solution appears to outperform the $\mathcal{O}(\varepsilon^3)$ WKB solution below the main bisector for small values of S and ε. This improvement becomes more appreciable as λ is increased due to the consistent reduction in the multiple-scale error.

Table 1. Exact and asymptotic solutions for $S=\lambda=10$ and $\varepsilon=10^{-4}$. Here, $y_0^{\mathrm{G}}=y_0^{\mathrm{C}}=y_0^{\mathrm{T}}$

x	y^{E}	y_0^{G}	y_0^{K}	y_2^{W}	y_1^{W}	y_0^{W}
0.50	0.0000008	0.0000008	0.0000008	0.0000008	0.0000008	0.0000008
0.55	0.0000062	0.0000062	0.0000060	0.0000062	0.0000062	0.0000060
0.60	0.0000133	0.0000132	0.0000128	0.0000132	0.0000132	0.0000128
0.65	-0.0000774	-0.0000774	-0.0000754	-0.0000773	-0.0000773	-0.0000754
0.70	-0.0007450	-0.0007451	-0.0007298	-0.0007443	-0.0007444	-0.0007298
0.75	-0.0030832	-0.0030832	-0.0030358	-0.0030808	-0.0030811	-0.0030356
0.80	-0.0070314	-0.0070308	-0.0069524	-0.0070275	-0.0070278	-0.0069521
0.85	-0.0018222	-0.0018203	-0.0018063	-0.0018214	-0.0018215	-0.0018062
0.90	0.0608180	0.0608212	0.0605377	0.0608038	0.0608049	0.0605368
0.95	0.3132358	0.3132386	0.3125648	0.3132022	0.3132047	0.3125627

be insensitive to λ. In addition, E appears to be insensitive to S for $\varepsilon<2\times10^{-4}$. As a result, the accuracy of Eq. (62) becomes nearly independent of variations in λ or S.

In Fig. 2d, all asymptotic errors are compared for $\lambda=2$ and $S=20,50,$ and 200. Despite its more compact expression, it is gratifying to note that the $\mathcal{O}(\varepsilon)$ multiple-scale solution for this case exhibits a smaller error than the $\mathcal{O}(\varepsilon^3)$ WKB solution. This is especially true for small values of S and ε. Additionally, the choice of $\lambda=6$ corresponds to an adverse case for y^{G}. While the WKB error remains unchanged, the trends are expected to favor the multiple-scale solution for which the error consistently diminishes with successive increases in λ. This is illustrated in Table 1 where exact and asymptotic solutions are compared side-by-side for $S=\lambda=10$ and $\varepsilon=10^{-4}$. In this example, y^{G} remains closer to y^{E} than the WKB solution of $\mathcal{O}(\varepsilon^3)$. In some cases, the agreement between true and asymptotic values is manifested in several significant digits.

VII. Example 2: Wave Propagation in Simulated Solid Rocket Motors

Several illustrative cases have appeared in the literature for which the present techniques apply. For $a_0=x^{-1}\sin(\frac{1}{2}\pi x^2)$, $a_1=1/x$, $b_0=-\pi\lambda\cos(\frac{1}{2}\pi x^2)$, $\lambda=2,4,6,\ldots$, $b_1=0$ and $c_0=1$, one obtains a problem that has received much attention in the works of Flandro and Roach,[41] Culick,[42] Chedevergne *et al.*,[27] and others.[16-18] In these studies, neither WKB nor GST solutions in the present form have been available. In this context, while a leading order GST solution is possible in light of Eq. (48), a formal WKB solution of Type II cannot be obtained in closed form. Even the Type I solution leads to a series expression because of the presence of $x^5\csc^5(\frac{1}{2}\pi x^2)$ in the integrand of Eq. (13). This impediment may be attributed, in part, to the need to integrate $2\xi^2S^{-1}c_0^3a_0^{-5}$ analytically, an often prohibitive operation, depending on the nonlinearity of a_0 (and c_0). Given these factors, one immediately realizes a distinct advantage of the CST approach: since Eq. (35) may be resolved through differentiation rather than integration of the $w(x)$ function, a closed-form CST result is not restricted to problems with coefficients that are amenable to integration. In the same vein, the GST approximation is relatively convenient in that Eq. (48) comprises no terms higher than a_0^{-3}. Consequently, provided that $w(x)$ is manageable, a closed-form CST approximation may be retrieved, but the same cannot be said of the WKB or GST solutions. Depending on the coefficients of Eq. (1), the level of difficulty due to integration will be low in GST's Eq. (48), moderate in WKB Type I's Eq. (13), and high in Type II's Eq. (18).

VIII. Example 3: Wave Propagation in Planar Enclosure

Our third example corresponds to an original case that arises in the context of an oscillatory wave inside a planar enclosure for which Eq. (1) is prescribed by $a_0=\tan\varphi$, $a_1=0$, $b_0=-\frac{1}{4}\pi\lambda\sec^2\varphi$, $\varphi\equiv\frac{1}{4}\pi x$, $b_1=0$ and $c_0=1$. These expressions lead to

$$\varepsilon y''+\tan\varphi\, y'+\left(iS-\tfrac{1}{4}\pi\lambda\sec^2\varphi\right)y=0;\qquad y'(0)=0,\qquad y(1)=1. \tag{74}$$

Following the procedure described by Majdalani,[1] the ensuing multiply-perturbed boundary-value problem is likely to exhibit three dissimilar scales: $x_0=x$, $x_1=x_{\mathrm{i}}$ and $x_2=x_{\mathrm{w}}$. To explore this possibility, the fundamental techniques outlined above will be implemented and compared. Furthermore, the parametric range that leads to an unconditionally bounded wave motion will be determined for each of the solutions that are susceptible to spurious singularities. This step is necessary due to the presence of three dimensionless parameters, ε, S and λ.

A. WKB Approximation

When Eq. (18) is applied to Eq. (74), intractable integrals appear in y^{K}. The Type II solution is hence ruled out. In contrast, the Type I approximation may be constructed straightforwardly using Eq. (13). One obtains

$$y^{\mathrm{W}} = (\tan\varphi)^{\lambda}\exp\Big[-\tfrac{2}{\pi}\xi\Big[\csc^2\varphi - 2 - \ln(\tfrac{1}{2}\csc^2\varphi)\Big] + \tfrac{2}{\pi}iS\Big(\ln(\tfrac{1}{2}\csc^2\varphi) + \varepsilon\Big\{\tfrac{1}{2}\pi(\lambda-\tfrac{1}{2})(1-\cot^2\varphi) + \xi\Big[(3-4\cos^2\varphi)\csc^4\varphi - 4 - 2\ln(\tfrac{1}{2}\csc^2\varphi)\Big]\Big\}\Big)\Big] + \mathcal{O}(\varepsilon) \tag{75}$$

Note that the leading-order term in the imaginary argument contains a small correction of order $\varepsilon S \sim S^{-1}$.

B. Traditional Multiple-Scale Solution

As alluded to in Sec. IV, the problem at hand admits three dissimilar scales. Because of the nonlinear scaling structure near the core, a traditional multiple-scale approach based on a combination of two or more linear scales proves to be infeasible. The traditional approach is thereby abandoned.

C. CST Approximation

Assuming that the scaling transformation of Eq. (20) holds, we let $x_0 = x$ and $x_1 = x_{\mathrm{c}} = \varepsilon(1-x)x^{-2}$. The composite variable defined as such serves to duplicate asymptotically both $x_{\mathrm{i}} = \varepsilon x^{-2}$ and $x_{\mathrm{w}} = \varepsilon(1-x)$ near $x = (0,1)$, respectively. Using the conceptual result of Eq. (35) at $\mathcal{O}(\varepsilon)$, we readily extract

$$y^{\mathrm{C}} = (\tan\varphi)^{\lambda}\exp\Big(-\xi\Big\{\tfrac{1}{4}\sec\varphi\csc^3\varphi\Big[\tfrac{3}{2} + 2\cos(2\varphi) + \tfrac{1}{2}\cos(4\varphi)\Big]\eta(x) - \eta(1)\Big\} + \tfrac{1}{4}\varepsilon\pi^2\lambda^2\Big\{\tfrac{1}{4}\sec\varphi\csc^3\varphi \times\Big[1 - \lambda^{-1}\cos(2\varphi)\Big]\eta(x) - \eta(1)\Big\} + \tfrac{2}{\pi}iS\Big\{\ln(\tfrac{1}{2}\csc^2\varphi) + \tfrac{1}{4}\pi^2\varepsilon(1-2\lambda)\Big[\tfrac{1}{2}\cot\varphi\csc^2\varphi\eta(x) - \eta(1)\Big]\Big\}\Big) \tag{76}$$

Three different solutions, namely, y^{i}, y^{w} and y^{C}, can be recovered from Eq. (76) depending on whether η_{i}, η_{w} or η_{c} are entered. From Eq. (41), the spatial length scales that need to be retrofitted into Eq. (76) consist of

$$\eta_{\mathrm{i}} = x/2;\ \ \eta_{\mathrm{w}} = (1-x);\ \ \text{and}\ \ \eta_{\mathrm{c}} = x(x-1)/(x-2) \tag{77}$$

Were it not for the conjecture in guessing the scales upfront, y^{C} could have been deemed, perhaps, the simplest to derive and the most illuminating with respect to the inner-core and near-wall approximations. By evaluating Eq. (76) with η_{c}, a composite CST expansion may be arrived at, specifically

$$y^{\mathrm{C}} = (\tan\varphi)^{\lambda}\exp\Big\{-\tfrac{1}{16}\xi\sec\varphi\csc^3\varphi\Big[6 + 8\cos 2\varphi + 2\cos 4\varphi - \pi^2\lambda S^{-2}\left(\lambda - \cos 2\varphi\right)\Big]\eta_{\mathrm{c}} + \tfrac{2}{\pi}iS\Big[\ln(\tfrac{1}{2}\csc^2\varphi) + \tfrac{1}{8}\pi^2\varepsilon(1-2\lambda)\eta_{\mathrm{c}}\cot\varphi\csc^2\varphi\Big]\Big\} \tag{78}$$

If we now turn our attention to the wave amplitude, $(\tan\varphi)^{\lambda}\exp\chi$, it may be seen that the growth of the wave is strongly controlled by the exponential argument,

$$\chi = -\xi\frac{(x-1)x}{16(x-2)\cos\varphi\sin^3\varphi}\Big[6 + 8\cos 2\varphi + 2\cos 4\varphi - \pi^2\lambda S^{-2}\left(\lambda - \cos 2\varphi\right)\Big] \tag{79}$$

Evidently, a spurious singularity can occur near $x = 0$ where

$$\chi \approx -\frac{2\xi}{\pi^3 x^2}\Big[16 - S^{-2}\pi^2\lambda(\lambda-1)\Big] + \frac{\xi}{\pi^3 x}\Big[16 - S^{-2}\pi^2\lambda(\lambda-1)\Big] + \ldots \tag{80}$$

Boundedness is therefore ensured so long as $16 - S^{-2}\pi^2\lambda(\lambda-1) \ge 0$ or $S \ge \tfrac{1}{4}\pi\sqrt{\lambda^2 - \lambda}$. For problems in which this condition is not fulfilled, the alternative is to lump, as usual, the $\mathcal{O}(S^{-2})$ part with the truncation order to obtain

$$\hat{y}^{\mathrm{C}} = \tan^{\lambda}\varphi\exp\Big[-\tfrac{1}{16}\xi\sec\varphi\csc^3\varphi\left(6 + 8\cos 2\varphi + 2\cos 4\varphi\right)\eta_{\mathrm{c}} + \tfrac{2}{\pi}iS\ln(\tfrac{1}{2}\csc^2\varphi) + \tfrac{1}{4}i\varepsilon S\pi(1-2\lambda)\eta_{\mathrm{c}}\cot\varphi\csc^2\varphi\Big] \tag{81}$$

D. GST Approximation

The GST solution may be viewed as the most straightforward of the group given that it does not require the CST's foreknowledge of the scales nor the WKB's distinguished limits and integrability requirement of high order terms. Based on Eq. (48), the GST expression may be written as

$$y^{\mathrm{G}} = (\tan\varphi)^{\lambda}\exp\Big\{-\tfrac{2}{\pi}\xi\Big[\csc^2\varphi - 2 - \ln(\tfrac{1}{2}\csc^2\varphi)\Big] + \tfrac{1}{4}\pi\varepsilon\lambda\Big[(1-\lambda)(1-\tfrac{1}{2}\csc^2\varphi) + (1+\lambda)\ln\cot\varphi\Big] + \tfrac{2}{\pi}iS\Big[\ln(\tfrac{1}{2}\csc^2\varphi) + \tfrac{1}{2}\pi\varepsilon(\lambda-\tfrac{1}{2})(1-\cot^2\varphi)\Big]\Big\} + \mathcal{O}(\varepsilon) \tag{82}$$

Unlike Example 1, Eq. (82) proves to be quite different from y^{C}. Nonetheless, it carries the same leading-order terms as y^{W}. In comparison to the latter, it contains small additional corrections, especially in its real argument,

that tend to enhance its accuracy. Furthermore, despite the dissimilarity between y^{G} and y^{C}, they both share the same exponential argument in their wave amplitude in the neighborhood of the origin. Physicality of Eq. (82) at $x=0$ is hence contingent on $S \geq \frac{1}{4}\pi\sqrt{\lambda^2-\lambda}$. Assuming that $S^{-2}=\mathcal{O}(\varepsilon)$ or smaller, a uniformly bounded representation may be given by

$$\tilde{y}^{G}=\tan^{\lambda}\varphi\exp\left\{-\tfrac{2}{\pi}\xi\left[\csc^2\varphi-2-\ln(\tfrac{1}{2}\csc^2\varphi)\right]+i\left[\tfrac{2}{\pi}S\ln(\tfrac{1}{2}\csc^2\varphi)+\varepsilon S(\lambda-\tfrac{1}{2})(1-\cot^2\varphi)\right]\right\}+\mathcal{O}(\varepsilon) \qquad (83)$$

E. Comparative Analysis

The absence of an exact solution for Eq. (74) is circumvented by numerical integration. We use Butcher's seventh-order Runge-Kutta technique in concert with shooting and linear superposition[1] to obtain a numerical solution that we label y^{N}. We find that a small step size of $\Delta x=10^{-6}$ is sufficient to ensure accuracy in all digits reported in y^{N}. By way of confirmation, we test the code by solving Example 1 and verifying that y^{N} coincides with y^{E} everywhere.

In Fig. 3, y^{N} is compared to y^{W}, y^{C} and y^{G}. Despite their dissimilar formulations, both multiple-scale solutions overlap on the graph. Due to reasons stated earlier, the agreement between y^{W} and y^{N} in Fig. 3a gradually depreciates in Figs. 3c and 3d as S is increased at constant ε. The multiple-scale expressions, however, remain more robust, being less sensitive to variations in S. When the perturbation parameter is decreased to $\varepsilon=10^{-3}$ (or beyond), the agreement with y^{N} is markedly increased. This is illustrated in Fig. 3d where all four solutions are shown to concur throughout the solution domain. In particular, it is interesting to note the agreement between numerics and asymptotics near the multiple wave peaks. This favorable behavior enables us to rely on the approximate formulations to accurately predict the wave depth, δ, as illustrated in Fig. 3d. Since δ is sensitive to small deviations, it can be used as a performance tool to gauge the level of agreement between numerics and asymptotics. Following classic theory, the wave's penetration depth δ is defined here as the distance from the porous wall to the point where the solution reaches 99% of its final value.

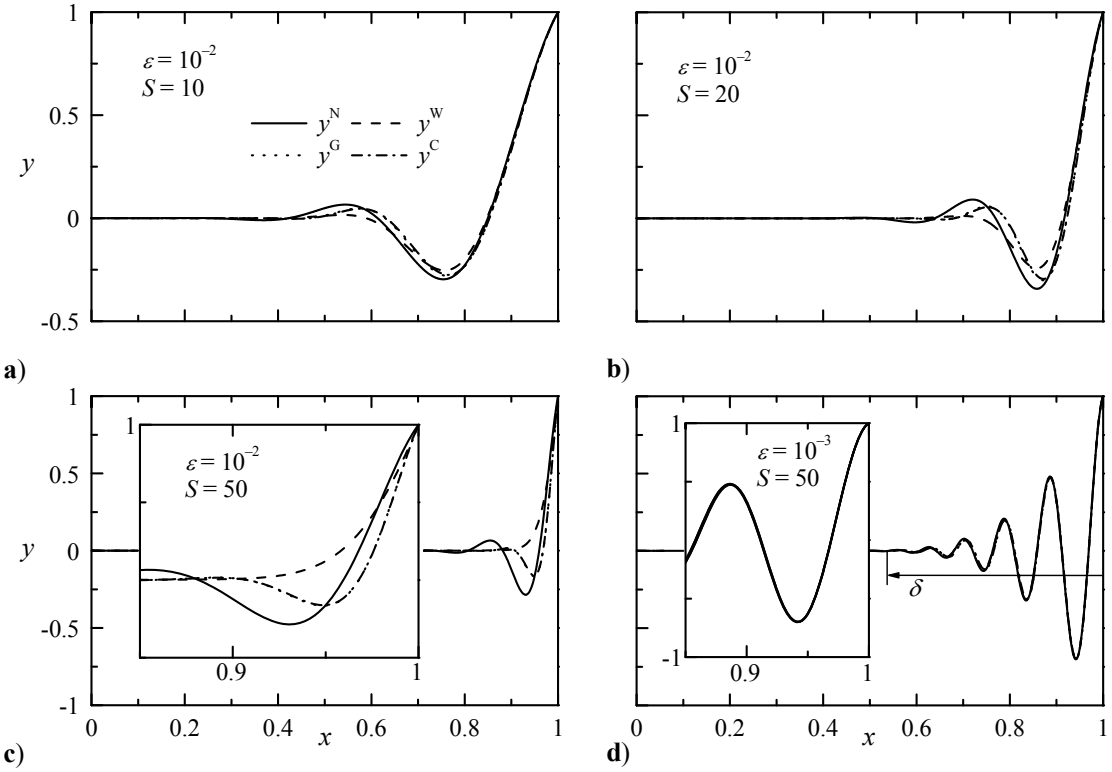

Figure 3. A comparison of numerical (y^{N}) with WKB (y^{W}) and multiple-scale approximations (y^{C} and y^{G}). For $\varepsilon=10^{-2}$ and $\lambda=2$, S is varied from a) 10, to b) 20 and c) 50. Results become visually confounded in d) where ε is decreased from 10^{-2} to 10^{-3} while keeping S constant. Also shown in d) is the wave depth, δ. As before, enlargements are shown in the insets.

1. Numerical vs. Asymptotic Wave Depths

In order to gain a better understanding of the inner scaling structure, the wave depths predicted by y^{W}, y^{G} and y^{C} are shown in Fig. 4 using $\varepsilon = 10^{-3}$. In addition to the uniformly valid y^{C}, we also show the inner-core y^{i} and near-wall y^{w} obtained through Eqs. (76) and (77). Our concern here is not so much with the uniformly valid solutions (which appear to concur over a wide range of ξ) as it is with the local approximations. In fact, for both $\lambda = 2$ in Fig. 4a and $\lambda = 4$ in Fig. 4b, the near-wall approximation y^{w} appears to offer an adequate representation as long as δ remains small. The same can be said of the inner-core approximation y^{i}. As expected, the latter provides an accurate prediction for δ near the core. Both y^{w} and y^{i} deteriorate as we distance ourselves away from the wall and the core, respectively. The accuracy that these local approximations offer can be attributed to the validity of the inner-core and near-wall scales in their particular spatial domains.

2. GST vs. CST Scaling Transformations

In retrospect, $s_{g}(x)$ may be determined from Eq. (51) and compared to Eq. (24). When this is performed, two relevant conclusions may be drawn. First, by systematically deriving s_{g} from the problem's solvability condition, the presence of nonlinearity in scaling constitution is formally ascertained. Second, s_{g} may be seen to resemble in spatial content the composite scale s_{c}. Both are shown in Fig. 5 along with the inner-core and near-wall scales. Note that s_{i} and s_{w} establish the upper and lower asymptotic limits of their uniformly valid counterparts.

3. Numerical Versus Asymptotic Error Analysis

The mechanics of characterizing the error behavior are identical to those of Example 1 except that y^{N} must now replace y^{E}. We find the results to be indispensable in evaluating the order of the error entailed in each formulation. The truncation order analysis is also instrumental in demonstrating the legitimacy of the corresponding

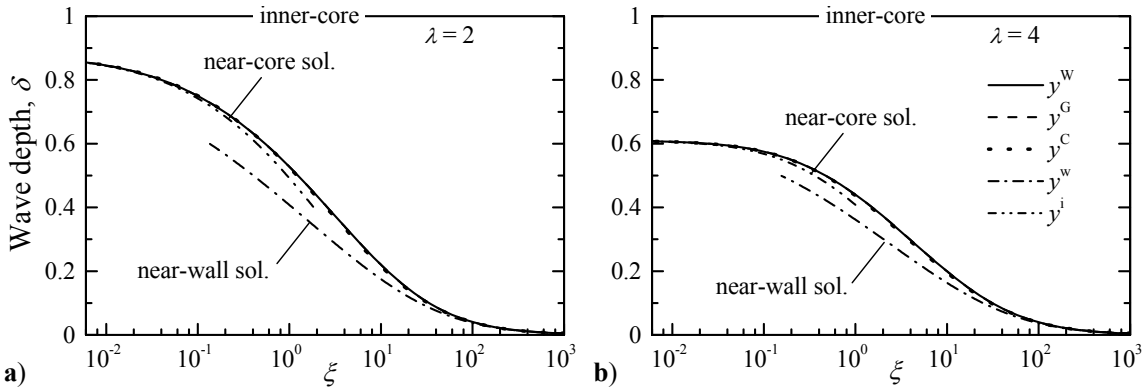

Figure 4. Wave depths of the oscillatory solutions as predicted by the various asymptotic equations for a) $\lambda = 2$ and b) $\lambda = 4$. The uniformly valid y^{W}, y^{G} and y^{C} coincide with the numerical solution (for $\varepsilon \le 10^{-3}$) to such a degree that their curves graphically overlap.

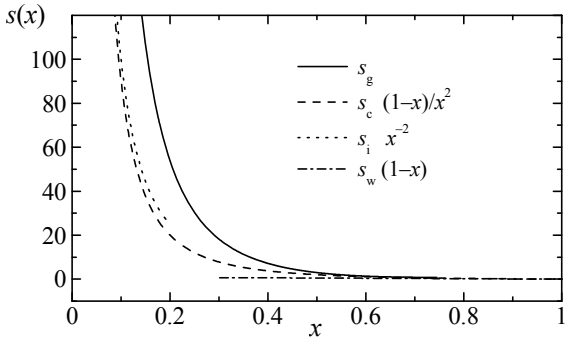

Figure 5. Spatial behavior of generalized-scale, composite-scale, inner-core, and near-wall variable transformations. Unlike the predefined spatial scales, s_{g} depends on S and λ. Here, it is shown for $S = \lambda = 2$.

approximations.[40] To that end, the absolute errors in y^{C}, y^{G} and y^{W} are plotted versus ε in Figs. 6a-c for three values of S and λ. Using the standard logarithmic form $E = K\varepsilon^{m}$, the error order m may be graphically discerned. We find that both CST and WKB errors exhibit a well-behaved asymptotic order in Figs. 6a and 6c. The GST error depreciates more rapidly in Fig. 6b as $m \to 2$ asymptotically in ε. Along similar lines, errors entailed in the multiple-scale approximations decrease with successive increases in λ. However, they seem to barely increase with S. This behavior does not mar the WKB error which has the advantage of being weakly dependent on S (as $\varepsilon \to 0$), and nearly insensitive to λ. When all three errors are compared for $\lambda = 6$ in Fig. 6d, the improved performance of y^{G} below the main bisector may be singled out. In addition to its higher rate of depreciation, the consistent reduction in the GST error at higher values of λ may be connected to the formal procedural steps that make use of information at the $\mathcal{O}(\varepsilon^{2})$ perturbation level while deriving an approximation for y^{G} at $\mathcal{O}(\varepsilon)$.

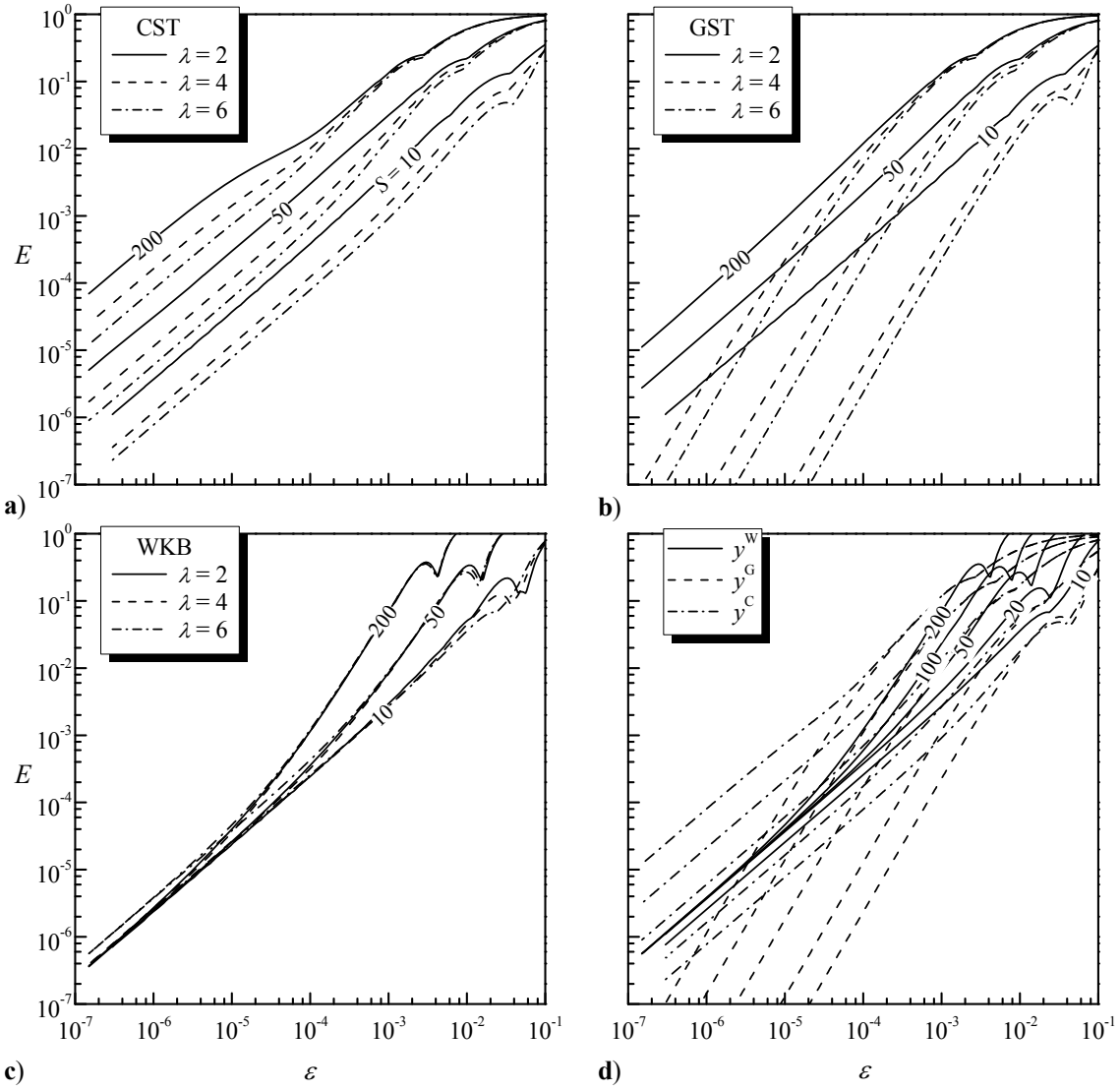

Figure 6. Plot of the absolute error versus ε at constant S. The errors in y^{C}, y^{G} and y^{W} are shown in a), b) and c) for $\lambda = 2,4$ and 6. Unlike a) and b), the error in the WKB solution does not decrease at higher integers. The one-term GST solution in b) exhibits an accelerated convergence rate caused by its error shifting from order 1 at $\lambda = 2$ to order 2 thereafter. When errors are compared in d) for $\lambda = 6$ and $S = 10,20,50,100$ and 200, the $\mathcal{O}(\varepsilon)$ GST solution appears to outperform both WKB and CST solutions below the bisector line. Thus, for small S or ε, the error in y^{G} outperforms that in y^{W}. This improvement becomes more appreciable as λ is increased due to the corresponding reduction in the multiple-scale error.

IX. Conclusions

In this article, three asymptotic techniques are applied to a singular, second-order, multiply-perturbed, boundary-value problem. With the exception of the WKB approach, the CST and GST formulations increase our repertoire of rational approximations for this particular class of ODEs. The startup equation is chosen with sufficient generality to make it applicable to physical settings arising in planar, cylindrical, and spherical geometries where oscillatory motion may be established. In this work, the three aforementioned techniques are thoroughly tested and compared using three independent benchmark cases.

In hindsight, the originality of the GST procedure may be attributed to its ability to provide the correct generalized-scaling transformation while seeking to observe the problem's solvability condition. In the same vein, we find the nonlinearity in the resulting scale to be attributable to the mathematical need for boundedness between two successive perturbation levels. In Example 1, the GST outcome precisely reproduces the result of the CST approximation. Being entirely conjecture-free, the formal solution emerging thereof is helpful in clarifying the failure of linear transformations. The presence of nonlinearity, though infrequent, may actually be anticipated in problems with overlapping dissipative and dispersive mechanisms. In fact, it does not constitute an unprecedented occurrence. According to Van Dyke,[43] a nonlinear transformation was first introduced by Munson[44] in his study of the vortical layer on an inclined cone. Therein, linear stretching was proved ineffective to the extent that an inner coordinate of the form $x_i = x^{\varepsilon}$ had to be conjectured.

The leading-order GST approximation exhibits several characteristic properties. Besides leading to a compact expression, it is shown to be (a) straightforward to derive, (b) accurate over a wide range of parameters, (c) more accurate with successive increases in (the eigenvalue) λ, (d) unaffected by distinguished limits, (e) useful in illuminating the problem's inner scales, (f) capable of accommodating an arbitrary scaling constituent, (g) of higher convergence rate, and (h) guesswork-free. The latter attributes distinguish the GST from the WKB technique. The WKB error, in comparison, (i) increases with λ, (ii) depends on the $\mathcal{O}(S)$ condition, (iii) offers no direct information about the scaling structure, (iv) exhibits a regular convergence rate, (v) requires the evaluation of harder integrals, and (vi) requires careful scaling before establishing its distinguished limits. The main advantage of the WKB solution lies in its gradual insensitivity to S as $\varepsilon \to 0$. The main setback in both WKB and GST procedures stands in their potential failure, however remote, to generate closed-form expressions. This is due to their reliance on the integrability of the variable coefficients that define the ODE in question.

The CST approach, on the other hand, is based on the systematic identification, matching, and presetting of the scales. It shares the (a) through (f) features stated above. In addition, it enables us to obtain locally valid approximations such as those that apply to the inner-core and near-wall regions. In so doing, however, it may not exhibit an accelerated convergence rate and will often require guesswork or trial in determining the scales. Its main advantage lies in its minimal requirement for integration. The CST approach can therefore present a unique analytical platform in the event when both WKB and GST solutions prove intractable. Both Examples 2 and 3 illustrate cases for which the WKB solution of Type II cannot be obtained in closed form. Countless intractable problems with intricate variable coefficients fall under this category. Despite its reliance on the unconventional step of first reducing the scales, the CST solution employs the standard multiple-scale notion that suggests defining the variable transformations before differentiating. In the GST procedure, the scales are, instead, determined at the conclusion of the analysis. Interestingly, despite the blatant dissimilarities between the CST and GST expressions in Example 3, they both share the same asymptotic behavior in their wave amplitude when evaluated at the origin.

In closing, we return to Example 1 and note that, aside from being useful in verifying the accuracy of the conceptual formulations, it also serves to extend and provide one exact and two asymptotic solutions to a study introduced previously by Majdalani.[4,5] From a perturbative standpoint, the attendant discussion clarifies and, in a way, justifies the paradigm adopted before in selecting nonlinear scales.[1] Futuristically, it is hoped that the added freedom furnished in the GST approach will be further explored in problems with two or more dissimilar scales. We also trust that a higher order expansion of the generalized scale will be tested in the treatment of similar problems involving jointly dispersive and dissipative waves.

Acknowledgments

This project was completed with support from the National Science Foundation through grant No. CMMI-0928762.

References

[1]Majdalani, J., "A Hybrid Multiple Scale Procedure for Boundary Layers Involving Several Dissimilar Scales," *Journal of Applied Mathematics and Physics (ZAMP),* Vol. 49, No. 6, 1998, pp. 849-868. doi: 10.1007/s000330050126

[2]Majdalani, J., and Van Moorhem, W. K., "Improved Time-Dependent Flowfield Solution for Solid Rocket Motors," *AIAA Journal,* Vol. 36, No. 2, 1998, pp. 241-248. doi: 10.2514/2.7507

[3]Majdalani, J., and Roh, T. S., "The Oscillatory Channel Flow with Large Wall Injection," *Proceedings of the Royal Society of London, Series A,* Vol. 456, No. 1999, 2000, pp. 1625-1657. doi: 10.1098/rspa.2000.0579

[4]Majdalani, J., "Vortical and Acoustical Mode Coupling inside a Two-Dimensional Cavity with Transpiring Walls," *Journal of the Acoustical Society of America,* Vol. 106, No. 1, 1999, pp. 46-56. doi: 10.1121/1.428032

[5]Majdalani, J., "Asymptotic Formulation for an Acoustically Driven Field inside a Rectangular Cavity with a Well-Defined Convective Mean Flow Motion," *Journal of Sound and Vibration,* Vol. 223, No. 1, 1999, pp. 73-95. doi: 10.1006/jsvi.1998.2137

[6]Wasistho, B., Balachandar, S., and Moser, R. D., "Compressible Wall-Injection Flows in Laminar, Transitional, and Turbulent Regimes: Numerical Prediction," *Journal of Spacecraft and Rockets,* Vol. 41, No. 6, 2004, pp. 915-924. doi: 10.2514/1.2019

[7]Chedevergne, F., Casalis, G., and Majdalani, J., "DNS Investigation of the Taylor-Culick Flow Stability," AIAA Paper 2007-5796, July 2007.

[8]Majdalani, J., Flandro, G. A., and Roh, T. S., "Convergence of Two Flowfield Models Predicting a Destabilizing Agent in Rocket Combustion," *Journal of Propulsion and Power,* Vol. 16, No. 3, 2000, pp. 492-497. doi: 10.2514/2.5595

[9]Haselbacher, A., Najjar, F. M., Massa, L., and Moser, R. D., "Slow-Time Acceleration for Modeling Multiple-Time-Scale Problems," *Journal of Computational Physics,* Vol. 229, No. 2, 2010, pp. 325-342. doi: 10.1016/j.jcp.2009.09.029

[10]Stewart, D. S., Tangy, K. C., Yoo, S., Brewster, Q., and Kuznetsovy, I. R., "Multi-Scale Modeling of Solid Rocket Motors: Time Integration Methods from Computational Aerodynamics Applied to Stable Quasi-Steady Motor Burning," AIAA Paper 2005-0357, January 2005.

[11]Fabignon, Y., Dupays, J., Avalon, G., Vuillot, F., Lupoglazoff, N., Casalis, G., and Prévost, M., "Instabilities and Pressure Oscillations in Solid Rocket Motors," *Journal of Aerospace Science and Technology,* Vol. 7, No. 3, 2003, pp. 191-200. doi: 10.1016/S1270-9638(02)01194-X

[12]Venugopal, P., Najjar, F. M., and Moser, R. D., "Numerical Simulations of Model Solid Rocket Motor Flows," AIAA Paper 2001-3950, July 2001.

[13]Venugopal, P., Najjar, F. M., and Moser, R. D., "DNS and LES Computations of Model Solid Rocket Motors," AIAA Paper 2000-3571, July 2000.

[14]Venugopal, P., Moser, R. D., and Najjar, F. M., "Direct Numerical Simulation of Turbulence in Injection-Driven Plane Channel Flows," *Physics of Fluids,* Vol. 20, No. 10, 2008, pp. 105103-22. doi: 10.1063/1.2963137

[15]Majdalani, J., and Rienstra, S. W., "Two Asymptotic Forms of the Rotational Solution for Wave Propagation inside Viscous Channels with Transpiring Walls," *Quarterly Journal of Mechanics and Applied Mathematics,* Vol. 55, No. 1, 2002, pp. 141-162. doi: 10.1093/qjmam/55.1.141

[16]Majdalani, J., and Flandro, G. A., "The Oscillatory Pipe Flow with Arbitrary Wall Injection," *Proceedings of the Royal Society of London, Series A,* Vol. 458, No. 2023, 2002, pp. 1621-1651. doi: 10.1098/rspa.2001.0930

[17]Majdalani, J., and Van Moorhem, W. K., "A Multiple-Scales Solution to the Acoustic Boundary Layer in Solid Rocket Motors," *Journal of Propulsion and Power,* Vol. 13, No. 2, 1997, pp. 186-193.

[18]Majdalani, J., "The Boundary Layer Structure in Cylindrical Rocket Motors," *AIAA Journal,* Vol. 37, No. 4, 1999, pp. 505-508.

[19]Majdalani, J., "Multiple Asymptotic Solutions for Axially Travelling Waves in Porous Channels," *Journal of Fluid Mechanics,* Vol. 636, No. 1, 2009, pp. 59-89. doi: 10.1017/S0022112009007939

[20]Barron, J., Majdalani, J., and Van Moorhem, W. K., "A Novel Investigation of the Oscillatory Field over a Transpiring Surface," *Journal of Sound and Vibration,* Vol. 235, No. 2, 2000, pp. 281-297. doi: 10.1006/jsvi.2000.2920

[21]Beddini, R. A., "Injection-Induced Flows in Porous-Walled Ducts," *AIAA Journal,* Vol. 24, No. 11, 1986, pp. 1766-1773. doi: 10.2514/3.9522

[22]Beddini, R. A., and Roberts, T. A., "Turbularization of an Acoustic Boundary Layer on a Transpiring Surface," *AIAA Journal,* Vol. 26, No. 8, 1988, pp. 917-923. doi: 10.2514/3.9991

[23]Hino, M., Sawamoto, M., and Takasu, S., "Experiments on Transition to Turbulence in an Oscillatory Pipe Flow," *Journal of Fluid Mechanics,* Vol. 75, No. 2, 1976, pp. 193-207. doi: 10.1017/S0022112076000177

[24]Hino, M., Kashiwayanagi, M., Nakayama, A., and Hara, T., "Experiments on the Turbulence Statistics and the Structure of a Reciprocating Oscillatory Flow," *Journal of Fluid Mechanics,* Vol. 131, No. 1, 1983, pp. 363-400. doi: 10.1017/S0022112083001378

[25]Hino, M., Fukunishi, Y., and Meng, Y., "Experimental Study of a Three-Dimensional Large-Scale Structure in a Reciprocating Oscillatory Flow," *Fluid Dynamics Research,* Vol. 6, 1990, pp. 261-275.

[26]Abu-Irshaid, E. M., Majdalani, J., and Casalis, G., "Hydrodynamic Stability of Rockets with Headwall Injection," *Physics of Fluids,* Vol. 19, No. 2, 2007, pp. 024101-11. doi: 10.1063/1.2434797

[27]Chedevergne, F., Casalis, G., and Féraille, T., "Biglobal Linear Stability Analysis of the Flow Induced by Wall Injection," *Physics of Fluids,* Vol. 18, No. 1, 2006, pp. 014103-14. doi: 10.1063/1.216052

[28]Berman, A. S., "Laminar Flow in Channels with Porous Walls," *Journal of Applied Physics,* Vol. 24, No. 9, 1953, pp. 1232-1235. doi: 10.1063/1.1721476

[29]King, J. R., and Cox, S. M., "Asymptotic Analysis of the Steady-State and Time-Dependent Berman Problem," *Journal of Engineering Mathematics,* Vol. 39, No. 1, 2001, pp. 87-130. doi: 10.1023/A:1004824527547

[30]Zaturska, M. B., Drazin, P. G., and Banks, W. H. H., "On the Flow of a Viscous Fluid Driven Along a Channel by Suction at Porous Walls," *Fluid Dynamics Research,* Vol. 4, No. 3, 1988, pp. 151-178. doi: 10.1016/0169-5983(88)90021-4

[31]Berman, A. S., "Laminar Flow in an Annulus with Porous Walls," *Journal of Applied Physics,* Vol. 29, No. 1, 1958, pp. 71-75. doi: 10.1063/1.1722948

[32]Hasebe, M., Hino, M., and Hoshi, K., "Flood Forecasting by the Filter Separation AR Method and Comparison with Modeling Efficiencies by Some Rainfall-Runoff Models," *Journal of Hydrology,* Vol. 110, No. 1-2, 1989, pp. 107-136. doi: 10.1016/0022-1694(89)90239-4

[33]Yuan, S. W., "Further Investigation of Laminar Flow in Channels with Porous Walls," *Journal of Applied Physics,* Vol. 27, No. 3, 1956, pp. 267-269. doi: 10.1063/1.1722355

[34]Bender, C. M., and Orszag, S. A., *Advanced Mathematical Methods for Scientists and Engineers*, McGraw-Hill, New York, 1978.

[35]Murdock, J., "Validity of the Multiple Scale Method for Very Long Intervals," *Journal of Applied Mathematics and Physics (ZAMP),* Vol. 47, No. 5, 1996, pp. 760-789. doi: 10.1007/BF00915274

[36]Murdock, J., *Perturbations: Theory and Methods*, John Wiley, New York, 1991.

[37]Nayfeh, A. H., *Perturbation Methods*, John Wiley, New York, 1973.

[38]Majdalani, J., "On the Multiplicity of Planar Solutions for Axially Traveling Waves in Simulated SRMs," AIAA Paper 2009-4978, August 2009.

[39]Abramowitz, M., and Stegun, I. A., *Handbook of Mathematical Functions*, National Bureau of Standards, New York, 1964.

[40]Bosley, D. L., "A Technique for the Numerical Verification of Asymptotic Expansions," *SIAM Review,* Vol. 38, No. 1, 1996, pp. 128-135. doi: 10.1137/1038006

[41]Flandro, G. A., and Roach, R. L., "Effects of Vorticity Production on Acoustic Waves in a Solid Propellant Rocket," Air Force Office of Scientific Research, AFOSR Final Rept. 2060 FR, Bolling AFB, DC, October 1992.

[42]Culick, F. E. C., "Rotational Axisymmetric Mean Flow and Damping of Acoustic Waves in a Solid Propellant Rocket," *AIAA Journal,* Vol. 4, No. 8, 1966, pp. 1462-1464. doi: 10.2514/3.3709

[43]Van Dyke, M., *Perturbation Methods in Fluid Mechanics*, The Parabolic Press, Stanford, CA, 1975.

[44]Munson, A. G., "The Vortical Layer on an Inclined Cone," *Journal of Fluid Mechanics,* Vol. 20, No. 4, 1964, pp. 625-643. doi: 10.1017/S0022112064001434